1-1-2015

3806 Ma Isua rhyolites and dacites affected by low temperature Eoarchaean surficial alteration: Earth's earliest weathering

Allen Phillip Nutman
University of Wollongong, anutman@uow.edu.au

Vickie C. Bennett
Australian National University, vickie.bennett@anu.edu.au

Allan Chivas
University of Wollongong, toschi@uow.edu.au

Clark R. L Friend
Gendale, UK

Xiao-Ming Liu
Northwestern University

See next page for additional authors

3806 Ma Isua rhyolites and dacites affected by low temperature Eoarchaean surficial alteration: Earth's earliest weathering

Abstract

This paper reports evidence for Earth's oldest-recognised low temperature alteration, at ~3800 Ma. Potassic felsic schists with a protolith age of 3806 ± 2 Ma form a ~30 km long unit in the amphibolite facies, deformed, Isua supracrustal belt (West Greenland). At a single locality, boudinaged layers (nodules) within the schists are low strain zones: they are fine-grained, weakly feldspar-phyric, contain quartz amygdules and have fiamme-like structures, all supporting a volcanic protolith. The nodules and surrounding schistose matrix contain abundant, 100-50 μm, euhedral, oscillatory zoned 3806 Ma zircons. The rare earth patterns of the zircons indicate crystallisation was magmatic. Some zircons contain axial lobate voids indicating that they grew at low pressure as the magma exsolved a fluid. Ti-in-zircon thermometry indicates crystallisation temperatures of 750-650 °C. Taken together, these zircon features indicates growth at eutectic temperatures in a hypabyssal chamber as the magma was exsolving a fluid phase. The magmatic zircons have εHf initial values of ~0 and δ18OVSMOW of +5.0‰ (Hiess et al., 2009), showing that the source of the volcanic rocks was devoid of assimilated markedly older or weathered crustal material, and probably essentially juvenile. In contrast, the whole rock δ18OVSMOW values are elevated at +14.7 to +16.2‰, indicative of superimposed low-temperature alteration processes. The nodules and matrix schists have non-igneous bulk compositions, exemplified by strong enrichment in K2O and depletion in Na2O. They are depleted in Sr, have no negative Eu anomalies, but have high Rb/Sr, with an Rb-Sr age of 3760 ± 140 Ma (Jacobsen and Dymek, 1988). This indicates that the alteration involving strong degradation of plagioclase occurred in the Eoarchaean. Trace element compositions and establishment of alteration vectors suggest the protoliths were likely rhyolitic and dacitic in composition. The strongest-modified matrix schist compositions contain biotite ± calcite ± dolomite with increase in MgO relative to the nodules, which indicates early magnesian carbonate growth. The whole-rock chemistry, decoupling of the igneous zircon and whole-rock oxygen isotope signatures and the Rb-Sr dating indicate that after eruption, the 3806 Ma felsic volcanic rocks underwent Eoarchaean low-temperature potassic alteration with weathering and groundwater circulation the most likely process. The geochemistry of the Isua felsic schists is compared with that of better-preserved volcanic rocks where the alteration conditions are known. This suggests a subaerial environment. The carbonatisation of the Isua felsic schists demonstrates drawdown of atmospheric CO2 into rocks made porous by the weathering.

Disciplines

Medicine and Health Sciences | Social and Behavioral Sciences

Publication Details

Nutman, A. P., Bennett, V. C., Chivas, A. R., Friend, C. R. L., Liu, X. & Dux, F. W. (2015). 3806 Ma Isua rhyolites and dacites affected by low temperature Eoarchaean surficial alteration: Earth's earliest weathering. Precambrian Research, 268 323-338.

Authors

Allen Phillip Nutman, Vickie C. Bennett, Allan Chivas, Clark R. L Friend, Xiao-Ming Liu, and Florian Dux

3806 Ma Isua rhyolites and dacites affected by low temperature Eoarchaean surficial alteration: Earth's earliest weathering

Allen P. Nutman [a,b], Vickie C. Bennett [c], Allan R. Chivas [a], Clark R.L. Friend [d], Xiao-Ming Liu [e], Florian W. Dux [a]

Published in Precambrian Research (2015) volume 268, pages 323-338

[a] GeoQuEST Research Centre, School of Earth & Environmental Sciences, University of Wollongong, Wollongong, NSW 2522, Australia

[b] Beijing SHRIMP Centre, Chinese Academy of Geological Sciences, 26, Baiwanzhuang Road, Beijing, 100037 China

[c] Research School of Earth Sciences, Australian National University, Canberra, ACT 0200, Australia

[d] Glendale, Tiddington, Oxon, OX9 2LQ, UK

[e] State Key Laboratory for Continental Dynamics, Department of Geology, Northwestern University, Xi'an, 710069, China

email: anutman@uow.edu.au

Abstract

This paper reports evidence for Earth's oldest-recognised low temperature alteration, at ~3800 Ma. Potassic felsic schists with a protolith age of 3806±2 Ma form a ~30 km long unit in the amphibolite facies, deformed, Isua supracrustal belt (West Greenland). At a single locality, boudinaged layers (nodules) within the schists are low strain zones: they are fine-grained, weakly feldspar-phyric, contain quartz amygdules and have fiamme-like structures, all supporting a volcanic protolith.

The nodules and surrounding schistose matrix contain abundant, 100-50 μm, euhedral, oscillatory zoned 3806 Ma zircons. The rare earth patterns of the zircons indicate crystallisation was magmatic. Some zircons contain axial lobate voids indicating that they grew at low pressure as the magma exsolved a fluid. Ti-in-zircon thermometry indicates crystallisation temperatures of 750-650°C. Taken together, these zircon features indicates growth at eutectic temperatures in a hypabyssal chamber as the magma was exsolving a fluid phase. The magmatic zircons have ε_{Hf} initial values of ~0 and $\delta^{18}O_{VSMOW}$ of +5.0‰ (Hiess et al., 2009), showing that the source of the volcanic rocks was devoid of assimilated markedly older or weathered crustal material, and probably essentially juvenile. In contrast, the whole rock $\delta^{18}O_{VSMOW}$ values are elevated at +14.7 to +16.2‰, indicative of superimposed low-temperature alteration processes.

The nodules and matrix schists have non-igneous bulk compositions, exemplified by strong enrichment in K_2O and depletion in Na_2O. They are depleted in Sr, have no negative Eu anomalies, but have high Rb/Sr, with an Rb-Sr age of 3760±140 Ma (Jacobsen and Dymek, 1988). This indicates that the alteration involving strong degradation of plagioclase occurred in the Eoarchaean. Trace element

compositions and establishment of alteration vectors suggest the protoliths were likely rhyolitic and dacitic in composition.

The strongest-modified matrix schist compositions contain biotite ± calcite ± dolomite with increase in MgO relative to the nodules, which indicates early magnesian carbonate growth. The whole-rock chemistry, decoupling of the igneous zircon and whole-rock oxygen isotope signatures and the Rb-Sr dating indicate that after eruption, the 3806 Ma felsic volcanic rocks underwent Eoarchaean low-temperature potassic alteration with weathering and groundwater circulation the most likely process. The geochemistry of the Isua felsic schists is compared with that of better-preserved volcanic rocks where the alteration conditions are known. This suggests a subaerial environment, probably without heavy rainfall. The carbonatisation of the Isua felsic schists demonstrates drawdown of atmospheric CO_2 into rocks made porous by the weathering.

Keywords: Eoarchaean weathering, Oxygen isotopes, Eoarchaean felsic volcanic rocks, CO_2 drawdown, biomediation

1. Introduction

In this study we show that the protoliths of a distinct unit of deformed, amphibolite facies potassic quartzo-feldspathic schists dated at 3806±2 Ma from the Isua supracrustal belt of southern West Greenland (Fig. 1) were rhyolites and dacites, possibly including ignimbritic varieties, that shortly after eruption were affected by intense Eoarchaean low-temperature potassic alteration, and overprinted by variable amounts of early dolomitisation. At ~3800 Ma, near the beginning of the geological record, evidence for low temperature alteration / weathering leading to potassic alteration with CO_2 drawdown from the atmosphere indicates that these surficial processes can be recognised across almost 4 billion years of Earth history. Constraints on the ~3800 Ma environment and the possible role of biomediation associated with the alteration are discussed.

2. Geology of the Isua supracrustal belt

Within the Eoarchaean ~3000 km^2 Itsaq Gneiss Complex of southern West Greenland (Nutman et al., 1996, 2013) the largest supracrustal rock unit is the ~35 km long and up to 2.5 km wide amphibolite facies Isua supracrustal belt (Fig. 1). The belt is bounded by metaplutonic complexes, with that on the north being dominated by 3700-3690 Ma tonalite protoliths and 3650-3640 Ma granite sheets, and that to the south being dominated by 3820-3795 Ma tonalite protoliths (Nutman et al., 1993, 1996, 1997, 2000; Crowley et al., 2002; Crowley, 2003; Nutman & Friend, 2009). The southern part of the belt is intruded by ~3800 Ma tonalite sheets which were emplaced into already deformed volcanic and sedimentary rocks (Nutman et al., 1996, 1997, Crowley, 2003). To the west, the belt is in tectonic contact with Mesoarchaean gneisses and supracrustal rocks (Nutman and Friend, 2009), whereas eastwards it is coverage by the Inland Ice.

With uncertainties of ≤ ± 10 Ma, SHRIMP U-Pb zircon dating demonstrates that the Isua supracrustal belt contains rocks varying in age by ~100 million years. The southern part is dominated by ~3800 Ma rocks, whereas the northern and central portions consist of ~3700 Ma rocks (Fig. 1; Nutman et al., 1996, 1997; Nutman and Friend, 2009, and references therein). Between the 3800 and 3700 Ma portions of the belt there is the *dividing sedimentary unit*, which contains 3940-3760 Ma detrital zircons (Nutman and Friend, 2009; Nutman et al., 2009). This dividing sedimentary unit was interpreted to have an unconformity at its southern edge and its northern edge is an Eoarchaean mylonite, separating it from the ~ 3700 Ma terrane to the north (Nutman and Friend, 2009; Nutman et al., 2009). Therefore, it has been proposed that the ~3800 and 3700 Ma terranes evolved separately from each other and were tectonically juxtaposed before 3660 Ma, the age of the first igneous intrusions common to both terranes (Nutman et al., 1997, 2002, 2009; Crowley, 2003).

The dominant lithologies within both segments of the belt are similar, comprising amphibolites derived from basaltic, picritic and boninitic protoliths (the latter in the ~ 3700 Ma sequence only), felsic volcanic and sedimentary rocks and chemical sedimentary rocks, particularly chert and banded iron formation (BIF; e.g., Allaart, 1976; Nutman et al., 1984, 2007, 2009, 2010, 2013; Komiya et al., 1999; Polat et al., 2002; Polat and Hofmann 2003, Bolhar et al., 2004, 2005; Furnes et al., 2007; Jenner et al., 2009). Plutonic mafic rocks are much less common within the belt, but include some gabbros and ultramafic rocks that were derived from cumulates in layered gabbro intrusions (e.g., Dymek et al, 1988) and from the upper mantle (Friend and Nutman, 2011).

Most of the Isua supracrustal belt was strongly deformed in the Eoarchaean but only weakly deformed in the Neoarchaean as displayed by the contrasting degree of strain in the ~ 3500 Ma Ameralik dykes and their country rocks (e.g. Nutman 1986;

Nutman et al., 2004). This means that the compositional layering in the volcanic and sedimentary rocks is mostly of transposed tectonic origin (Nutman et al., 1986, 1996, 2002, 2007; Myers, 2001). Thus primary volcanic and sedimentary structures have survived in only a few places. The commonest relict structures are pillows within mafic rocks, graded layering in felsic volcano-sedimentary rocks and layering in banded iron formation (e.g., Nutman et al., 1984; 1997, 2007; Komiya et al., 1999; Solvang, 1999; Furnes et al., 2007). In this paper we discuss the origin and chemical modification of a felsic schist unit within the ~3800 Ma southern portion of the belt.

3. Geology of the ~3800 Ma felsic schist unit

3.1. Previous studies

Within the Isua supracrustal belt's southern ~3800 Ma segment, a potassic felsic schist unit is continuous for almost 30 km (Fig. 1). Its dominant mineralogy is quartz + K-feldspar + biotite ± muscovite ± plagioclase ± tremolite ± carbonate ± garnet. Strain is generally high, such that in most places layering in the unit is entirely tectonic (Fig. 2A). However, graded layering is preserved within it locally (Fig. 4a in Nutman et al., 1984). Much debated are features found in the core of a steeply plunging parasitic fold in the central segment of the unit on the eastern shores of the lake with an altitude 678 m, where the unit features prolate nodular structures up to 1 m long set in a more strongly eroded matrix (Fig. 2B). During the early exploration of the belt (Allaart, 1976), these structures were interpreted as acid volcanic bombs. Based on this volcanic interpretation, the nodular structures were the target of the first U-Pb zircon geochronology on Isua supracrustal belt rocks, with bulk analysis and small fraction techniques giving upper concordia intercept ages of 3824^{+12}_{-9} and 3813^{+21}_{-14} Ma (Michard-Vitrac et al., 1977; Baadsgaard et al., 1984). Compston et al. (1986) presented a SHRIMP weighted mean $^{207}Pb/^{206}Pb$ age of 3806±2 Ma (2σ). Subsequent

SHRIMP U-Pb zircon dating on continuations of this unit throughout the belt has yielded consistent ages within analytical error of each other from 3803±3 to 3807±6 Ma (Nutman et al., 1996, 2002; Hiess et al., 2009; supplementary data Table 1, and see Figure 1 for sample locations).

Throughout the 1970s the felsic schist unit was interpreted as an acid volcanic with large bombs preserved locally. Nutman et al. (1984) re-evaluated the unit, and concurred with an acid volcanic and/or volcano-sedimentary origin. Lines of evidence supporting this were the rare preservation of graded layering, and survival of microtextures resembling fiamme within the putative volcanic bombs (Fig. 3F; reproduced from Fig. 5 in Nutman et al., 1983). Nutman et al. (1984) also documented the deviation from igneous compositions, particularly high K_2O correlated with low Na_2O, which they interpreted as alteration soon after deposition. However, the 'bombs' were noted to occur only in the core of a fold and Nutman et al. (1984) reinterpreted them as tectonic boudins of more competent massive felsic rocks between layers carrying carbonate. In this paper we refer to these structures in a non-genetic sense as 'nodules'. The unit was re-evaluated again by Rosing et al. (1996) who concluded that it represents a strongly metasomatised, carbonated tonalite sheet intruded into the belt. Myers (2001) reinterpreted the unit as a strongly metasomatised series of mafic volcanic rocks.

Heiss et al. (2009) reported hafnium and oxygen isotopic data from aliquots of the same zircon separates from samples 248202 (matrix) and 248203 (nodule) that were used by Baadsgaard et al. (1984) and Compston et al. (1986) for zircon U-Pb dating. These zircons have initial ε_{Hf} values of +0.5 ±0.6 and +0.1±0.7 respectively, i.e. indistinguishable from CHUR. Their $\delta^{18}O_{VSMOW}$ values are mantle like, at +5.0±0.2 and +4.9±0.2‰ respectively. This indicates that the *source* of the magma

crystallising the zircons did not contain significantly older continental crust and that prior to partial melting the source had *not* been affected by low temperature alteration processes such as weathering.

Pope et al. (2012; their supporting information text) reported whole-rock and mineral oxygen isotope determinations on the 3806 Ma felsic unit, as part of a broader data set encompassing many lithologies of the Isua supracrustal belt and noted elevated $\delta^{18}O_{VSMOW}$ values up to +11‰ for the felsic unit rocks. They attributed the supra-mantle heavy oxygen signatures to a metasomatic influx of oxygen from the tonalitic domains adjacent to the Isua supracrustal belt. However, this explanation is not supported by the whole rock mantle-like oxygen (~ +6 to +8‰) of the tonalites (Baadsgaard et al., 1986a).

3.2. Field relationships

The felsic unit occurs throughout the length of the Isua supracrustal belt (Fig. 1) and lies within the core of a tectonically-partitioned early isoclinal fold (Nutman et al. 1984), corroborated by later work (Nutman and Friend 2009). To the south of the unit there are extensive metavolcanic mafic rocks that locally preserve north-facing relict pillow structures, towards the felsic schist unit (Nutman et al., 2002). Most of the mafic rocks are amphibolites with major and trace element chemistry resembling island arc tholeiites (Polat and Hoffman, 2003; Jenner et al., 2009). The amphibolites are cut by ~3800 Ma tonalite sheets, indicating their minimum age (Nutman et al., 1996; Crowley, 2003). High-Mg schists form discontinuous units along the belt and on most Isua geological maps are shown as ultramafic rocks. Chemically they are neither like upper mantle rocks nor basal parts of tholeiitic layered intrusions. Instead they chemically resemble olivine-rich picrites (Polat and Hofmann, 2003). Between the metavolcanic mafic rocks and the felsic schist unit there is a heterogeneous unit of

dolomitic marble, calc-silicate rocks and rare fuchsitic quartzite. To the north of the felsic unit this sequence is mirrored, such that along its northern margin there are marbles and calc-silicate rocks, and then metavolcanic mafic rocks with relict pillow structures indicating younging to the south, again towards the felsic schist unit (Nutman et al., 2002). The dolomitic marbles retain seawater-like rare-earth element + yttrium chemical signatures and the associated fuchsitic quartzites carry 3890-3810 Ma detrital zircons (Nutman et al., 1997; 2010), attesting to their sedimentary origins and a maximum depositional age of 3810 Ma. The calc-silicate rocks associated with the dolomites are interpreted as interlayered cherts and dolomites, which during metamorphism reacted and gave rise to diopside + quartz *or* diopside + dolomite rocks. Despite the strong tectonic disruption of these rocks, these relationships, geochemical, geochronological and isotopic data permit the following stratigraphic sequence to be proposed (Fig. 4): ≥3800 Ma arc-related metabasic rocks locally preserving pillow structures were overlain by ≤3810 Ma dolomites, cherts and detrital quartzite (with 3890-3810 detrital zircons) and then by the 3806 Ma felsic (schist) unit. The discontinuous nature of the high-Mg schist picritic rocks at the contact with the dolomites, cherts and detrital quartzites can be interpreted as (i) erosion below a (tectonised) unconformity or (ii) as a tectonic break that has excised some of the stratigraphy shown in Figure 4. The former is preferred, because of the continuity of the dolomite, chert and detrital quartzite unit along the belt.

Because of several superimposed Eoarchaean and Neoarchaean tectonothermal events, most of the felsic unit is very strongly deformed, such that its planar to lenticular layering is interpreted to be largely tectonic, with most protolith structures obliterated (Fig. 3A). However, at the locality on the eastern shore of lake with an altitude of 678 m (Fig. 1; Allaart, 1976; Nutman et al., 1984), nodular structures are preserved in a steeply-plunging parasitic fold core (Figs. 1, 3B). In this fold core the

rocks are strongly lineated, meaning the nodules Allaart (1976) interpreted as bombs are strongly prolate. The nodules are quartzo-feldspathic and largely devoid of carbonate, whereas their matrix bears considerable amounts of carbonate + biotite. Locally in the fold nose, "looking down" the lineation, the nodules appear to be concentrated into layers, with carbonate-bearing matrix between them (Fig. 2C). Following Nutman et al. (1984), this suggests that the nodules were derived from disrupted layers.

In the east of the belt (Fig. 1), finely layered, tectonised felsic schists with a U-Pb zircon date of 3806±3 Ma (Fig. 1, sample G05/15 in data repository Table 1) contain a low strain zone. In this zone (WGS84 datum 65°09.67'N 49°48.86'W) the rocks are interpreted as a breccia with a fine-grained felsic matrix (Fig. 2D). Breccia fragments are layered and rotated relative to each other. The matrix is felsic and equigranular. The breccia fragments are interpreted to have a volcanic or volcano-sedimentary protolith, whereas the matrix might represent hypabyssal intrusive material that disrupted the volcanic host. Possible graded layering has been proposed at scattered localities throughout the unit (Nutman et al., 1984), but overall >99% of the unit is so strongly deformed that original volcanic and sedimentary structures have been obliterated.

3.3. Whole-rock petrography

This study focuses on the nodules and their matrix at the locality on the shore of lake 678 m, in the vicinity of 65°05.76'N 50°00.39'W (Fig. 1). At the nodule locality all samples contain quartz + biotite + microcline ± muscovite in variable proportions. Carbonate together with biotite is widespread in the matrix. In some other parts of the felsic unit, abundant muscovite and/or small disseminated garnets are present. Most observations are from nodule sample G11/76 (Fig. 2B), which from geochemical

criteria (see below) shows the least severe modification of the protolith igneous composition. The nodules have a very fine-grained groundmass of feldspar + quartz with some biotite and patchy development of minor muscovite (Fig. 3A-E and H). In the matrix to the nodules, a fine-grained groundmass is also present but it has been overprinted by coarser-grained biotite + carbonate, forming irregular patches and veins. Even in the lowest strain areas, micas are aligned to give a weak foliation. Larger feldspar grains (up to 0.5 mm) are found in the matrix. Some consist entirely of alkali feldspar (Fig. 3B) whereas others are plagioclase variably replaced by alkali feldspar ± muscovite (Fig. 3C).The groundmass also contains ovoid features up to 2 mm across of polycrystalline quartz (Fig. 3D). These also occur in the carbonate-bearing matrix. Polycrystalline quartz also forms irregular–shaped polycrystalline aggregates up to 3 mm long (Fig. 3E). Noted in a 1980s study were fiamme-like structures in a nodule (Fig. 3F; this photomicrograph is reproduced from Nutman et al. (1983)). Biotite-rich clasts up to several mm long are also present (Fig. 3G).

The two commonest interpretations of these rocks are that (a) they are altered, metamorphosed felsic volcanic rocks (Allaart, 1976; Nutman et al., 1983, 1984) or (b) they are mylonitised and metasomatised tonalites (Rosing et al., 1996). There are key petrographic features that support the former volcanic interpretation, and negate the latter mylonitised tonalite interpretation. The ovoid quartz aggregates set in the very fine grained matrix (Fig. 3D) are interpreted as quartz amygdules, like similar features observed in some Isua metabasalts (e.g., Appel et al., 2009). The shape of these features points to locally low strain. This is texturally unlike quartz in high strain (mylonitic) rocks, where early kinematic quartz forms bands parallel to the mylonite fabric whereas late kinematic quartz forms discordant veins. Additionally, irregular polycrystalline quartz aggregates are found together with more euhedral feldspar

grains (Fig. 3E). The interpretation of this relationship is that the irregular polycrystalline quartz aggregates are (deformed) corroded quartz phenocrysts found with euhedral feldspar phenocrysts, residing within a (recrystallised) volcanic groundmass. Corroded quartz phenocrysts together with more euhedral feldspars are a common feature of acid volcanic rocks (Gill, 2011). The biotite-rich lenses shown in Figure 3G are orientated at a high angle to the long axis of a nearby altered plagioclase phenocryst. This again attests to low strain domains being preserved locally within these nodules, whereas the quartz amygdules, corroded quartz phenocrysts and possible fiamme argue against a deep-seated plutonic protolith. Therefore we interpret the felsic schist unit protoliths to be felsic volcanic rocks, including some vesicular, quartz + feldspar-phyric varieties, some of which might have been ignimbritic because of possible relict fiamme. The presence of the phenocrysts points to a two-stage cooling history for the magma. This can explain the presence of small (100-50 μm) euhedral, oscillatory-zoned igneous zircons, which probably grew during early slower cooling in a hypabyssal chamber.

4. Zircon petrography and geochemistry

4.1. Morphology

Zircons in 248203 (nodule) and 248202 (matrix) samples were U-Pb dated first by Baadsgaard et al. (1984) by bulk analysis and then by Compston et al. (1986) by SHRIMP at 3806 ± 2 Ma. Heiss et al. (2009) demonstrated that these zircons have $\varepsilon Hf_{(3800)}$ of ~0 and $\delta^{18}O_{VSMOW}$ of ~+5‰. Given the large amount of published isotopic data on these zircons, they were targeted for detailed petrographic study.

The zircons from both the nodule and the matrix display exactly the same petrographic features and are thus described together. They are typically pale yellow to translucent stubby prisms, between ~100-50 μm long, with a minority of longer grains

with higher aspect ratio. Cathodoluminescence (CL) imaging indicates that igneous micron-scale oscillatory zoning is widespread throughout the grains, with the zoning parallel to the grain exteriors (Figs. 5A, B and F). The exterior of the grains are euhedral to subhedral, with little evidence of rounding, and with no metamorphic overgrowths. The interior of the grains can display discontinuities between inner and outer domains of oscillatory zoning (Figs. 5A and F). However, the extensive SHRIMP U-Pb analysis of these grains (Compston et al., 1986; Heiss et al. 2009) found little dispersion in $^{207}Pb/^{206}Pb$ beyond that expected from analytical error alone. Therefore we interpret these discontinuities as magmatic resorption-regrowth features within the timeframe of the ± 2 million year uncertainty on the age of these zircons. These internal resorption and regrowth features are found in other purely magmatic zircon suites, such as in the 760 ka Bishop Tuff (Wark et al., 2007). Recrystallisation domains are developed sporadically with the grains, particularly close to inclusions of other minerals (Figs. 5B and E).

4.2. Inclusions in zircon

From transmitted, reflected and electron backscatter imaging, lobate and worm-like features are found in a sizeable minority of the zircons. Figure 5G (transmitted light) and H (reflected light) demonstrate an example of such a feature, trapped below the polished surface of the grain mount. Other examples are shown in Figures 5C and D, where they have been exposed at the surface of the mount. In C, the feature is a void that filled with epoxy resin during sample preparation, in D, the feature is an intact void within the zircon. Such lobate and worm-like features are never found within deep-seated plutonic zircons, but have been described from zircons crystallising from melts in surface or near-surface environments, where a separate H_2O-rich fluid phase was exsolving from silicate melt (I.S. Williams, personal

communication, 2014). Therefore we regard these lobate and worm-like features as evidence that the magmatic host of these zircons was crystallising at low pressure. There are also parallel-sided acicular features, which are now partly voids and partly occupied by muscovite and carbonate, and however, locally relict apatite has been detected within them (Fig. 5I). Additionally, in the case of sample G97/102 (Fig. 1) an apatite-shaped domain has been pseudomorphed by muscovite + galena (Fig. 5J; documented by Scanning Electron Microscope Energy Dispersive X-Ray Analysis (EDX)). This suggests these were once acicular apatite inclusions in the zircons, which were dissolved by post-magmatic fluids and then partly replaced by other phases. Dissolution of apatite inclusions from zircons and the infilling of the voids by other minerals is a very common feature of grains subjected to surficial environments (Rasmussen et al., 2011).

EDX analysis of nodule sample 248203 zircons documents that they contain inclusions of quartz + rutile, biotite (showing rutile exsolution), biotite + K-feldspar, quartz + K-feldspar and rare ilmenite and apatite (Figs. 5A, B, D and F). Particularly notable in the context of Ti-in-zircon thermometry is the occurrence of quartz + rutile in equilibrium within the zircons (Fig. 5B). Plagioclase inclusions, or alteration products thereof, were not detected. This differs from the inclusion suite of plagioclase + quartz + apatite + biotite + some K-feldspar that occurs in ~3800 Ma coarse-grained (plutonic) tonalite sample G97/18, approximately 15 km to the south (Fig. 1; Nutman et al., 1999, 2009), suggesting the magma composition of the nodule sample 248203 was different from, and probably more potassic (i.e. rhyolitic), than the regional ~3800 Ma tonalites.

4.3. Zircon trace-element geochemistry and Ti-in-zircon thermometry

Laser ablation ICP-MS analyses of zircons in samples 248203 (nodule) and 248202 (matrix) were undertaken at Northwestern University, Xi'an, employing a ~30 μm spot and following the trace-element analytical method outlined in Yuan et al. (2008). The REE, Th, U, Ti and P were analysed, the latter being to appraise the presence of any xenotime component in the analysed sites. Unknowns were calibrated to NIST610 glass; a few analyses of SL13 zircon run as unknowns gave a mean U abundance of 239 ppm, compared with the accepted value of 238 ppm. Data are summarised in Table 1 and the REE variation is portrayed in chondrite-normalised plots (Figs. 6A, B).

Analyses of the nodule and matrix zircons show identical chemistry, thus they are discussed together. All zircons have low P contents and high Th/U, which together with the presence of the oscillatory zoning visible in CL images indicates they are magmatic with minimal xenotime component present. There is strong fractionation of the REE, such that Yb and Lu have >1000 chondritic abundance, whereas La has mostly sub-chondritic abundance (Figs. 6A, B). A few analyses show slightly higher La abundance (up to x10 chondrite) with more subdued positive Ce anomalies and without increase in P (Table 1; Figs. 6A,B). The somewhat more La-enriched domains without P enrichment (no xenotime) suggest some hydrothermal influence (intermittent boiling?) during zircon growth (Hoskin, 2005). All analysed zircons display negative Eu anomalies, whereas the felsic schist unit whole-rock samples do not (Fig. 6C). This indicates that zircon grew in plagioclase-phyric magma.

Some of the zircon analyses show high Ti content (>20 ppm), suggesting micron-scale rutile and biotite inclusions contributed to the analyses. Therefore discussion of Ti-in-zircon abundance is restricted to analyses of zircon where the low Ti abundance suggests that it is only present in the zircon, *not* partially in inclusions. For these sites Ti abundance is from 2.4 to 13.5 ppm and well above quantification

limits (Table 1). The temperature of zircon crystallisation can be established by the Ti concentration of zircon in equilibrium with rutile and quartz (Watson and Harrison, 2005), a criterion met by sample 248203 and 248202 zircons. Using the Ferry and Watson (2007) recalibration of this thermometer ($\log(\text{Ti ppm}) = 5.711\text{-}4800/T\text{-}\log(aSiO_2)+\log(aTiO_2)$; with T = temperature in Kelvin), temperatures range from 627 to 789°C, suggesting zircon growth over a ~165°C range (Fig. 7). It is possible that the range is somewhat less (~130°C), if the two sites with the highest Ti also contain Ti-rich micro-inclusions. The low temperatures are compatible with zircon growth in an evolved, hydrous felsic melt at or close to eutectic conditions. This also agrees with the petrological evidence that the magma was exsolving a fluid as the zircons were crystallising.

5. Whole-rock geochemistry

5.1. Analytical methods

Eight analyses of the felsic unit undertaken with recent XRF major and ICP-MS trace element-methods are presented in Table 2. Samples were crushed using a TEMA chromium ring mill. Fused buttons were made for X-ray fluorescence (XRF) major-element analysis using pure metaborate flux. Pressed pellets for trace-element analysis were created by mixing ~5 g of the sample with a polyvinyl acetate (PVA) binder and pressed into an aluminium cup using a hydraulic hand press. Trace-element pressed pellets were then oven dried at 60°C for 12 hours. Whole-rock geochemical analysis was conducted using a SPECTRO XEPOS energy dispersive polarisation X-ray fluorescence spectrometer at the University of Wollongong. Laser-ablation ICP-MS trace element and REE analyses of samples 248203, G93/24, G04/68 and G04/69 were undertaken at the ANU using the method outlined in Friend et al. (2007). ICP-MS trace element and REE analyses of the other samples were undertaken at the

Queensland University of Technology, using similar methodology. These are augmented with a large number of analyses undertaken by XRF in the 1970s at the Geological Survey of Greenland, two of which were analysed for the REE by O'Nions and Pankhurst (1974; data in online supplementary Table 2 and see footnote of Table 2 in Nutman and Bridgwater (1986) for analytical methods on all these samples). The modern and old data are congruent, and some of the 1970s data are particularly useful because CO_2 was analysed, permitting chemical changes related to carbonation to be identified.

5.2. Alteration

Field and petrographic criteria show that the felsic schists underwent significant early post-magmatic alteration, which pre-dates the earliest tectonothermal events. In the major-element chemistry, the most obvious non-magmatic feature is the high K_2O (>10 wt% for some samples) coupled with <1 wt% Na_2O in most samples (Table 2; Fig. 8A). These trends are common in the low-temperature alteration of felsic volcanic rocks and tuffs and indicate replacement of alkali and plagioclase feldspars by K-feldspar (e.g., Rougvie and Sorensen, 2002 and references therein). The Rb-Sr variation in the felsic schists is also non-magmatic, with anomalously low Sr but similar Rb abundances compared to those in unaltered Eoarchaean felsic plutonic rocks (Fig. 8B). There is no significant difference in the REE distributions between nodules, their matrix and samples of layered schist (Fig. 6C), and there is no significant fractionation compared with Eoarchaean plutonic granites and tonalites (data in Nutman and Bridgwater, 1986; Nutman et al., 1999). This demonstrates that the process that added potassium or that which caused addition of carbonate did not disturb the magmatic REE chemistry to a degree detectable beyond the likely 10% uncertainties in the REE abundances. A singular feature is the very negative Sr

anomalies, without Eu anomalies (Fig. 9A). The lack of negative Eu anomalies argues against fractionation of plagioclase from the melts as the cause of the Sr signature. Therefore the depletion of Sr could be related to breakdown of plagioclase, with Sr (and Na, Ca) removal in solution. A similar signature is seen in other early Archaean volcanic rocks, such as ~3460 Ma Kittys Gap rocks of the Worrawoona Group, Pilbara craton (Fig. 9; Smithies et al., 2007).

Samples with the highest CO_2 content also show the highest MgO, CaO and MnO (Online supplementary Table 2; Figs. 8C, D). Assuming MgO and CaO abundances typical of unaltered granites (~1 wt% and 2 wt%, respectively) for the igneous protoliths, the vectors of MgO versus CaO and CO_2 indicate that the added carbonate was calcic dolomite or largely stoichiometric dolomite + some calcite (Figs. 8C, D).

In terms of the M (mafic igneous) – F (felsic igneous) – W (weathering) component diagram of Ohata and Arai (2007), non-altered ~3800 Ma calc-alkaline meta-plutonic rocks from south of Isua lie along the igneous trend (Fig. 10). Contrary to this, the felsic schists scatter across the field of weathered rocks. This expresses the variable and in some cases severe modification of the igneous protoliths. Samples with the highest CO_2 content or total volatiles (where CO_2 was not measured) also have the highest MgO + CaO contents, and are translated upwards towards the M (mafic igneous) apex of the plot (Fig. 10). The reason for this is that addition of MgO + CaO via dolomite makes these samples appear more mafic in this diagram. Samples that correspond to the weathering of dacite and weathering of rhyolite vectors (Fig. 10) have the lowest CO_2 or total volatile contents.

5.3. Igneous protoliths

The REE and HFSE are generally thought to be resistant to post-magmatic alteration in igneous volcanic systems on which regional metamorphism has been superimposed (e.g., Polat and Hofmann, 2003 and references therein). In the felsic schists, the LREE are enriched relative to HREE and the primitive mantle ($La/Yb_{(N)}$ from 17 to 38, relative to chondrite values of McDonough and Sun, 1995), and have negligible Eu anomalies (Fig. 6C).

In a trace-element spider-plot (Fig. 9A; normalised to primitive mantle values of McDonough and Sun, 1995), several likely igneous features are revealed, such as strong negative Ti, Nb and Ta anomalies, as seen in plutonic tonalites to the south (Fig. 9B). These features are likely to indicate suprasubduction magmatic systems, involving subcrustal retention of Ti, Nb and Ta during melt production (Nutman et al., 1999; Hoffmann et al., 2011; Friend and Nutman, 2011). Using Nb and Y (Fig. 8E), elements likely to have been least modified by the post igneous processes, the felsic schist samples plot well within the volcanic arc granites field of Pearce et al. (1984), and the eclogite-melting field of Archaean tonalites in the La/Yb versus Yb diagram of Martin (1994; Fig. 8F). Therefore the felsic schist igneous protoliths are regarded to have formed from arc-related, evolved, siliceous magmas.

In the MFW diagram, nodule samples with the lowest CO_2 or total volatile content form scattered arrays, one between unaltered rhyolites and ‘W’ and the other between unaltered dacites and ‘W’ (Fig. 10). Samples plotting in the weathering of rhyolite trend are all from the single nodule locality on the shores of lake 678 m (Fig. 1), including samples 248203, G11/76 and G11/77. Of these, sample G11/76 plots closest to granite/rhyolite which would explain why relict igneous petrographic features are more recognisable in this sample compared with others. Therefore we contend that the 3806 Ma felsic schist unit contained both rhyolite (*sensu* the broad category of Le Maitre et al., 2005) and dacite protoliths.

6. Whole-rock oxygen isotopes

6.1. Analytical method

Oxygen for isotopic analysis, at the University of Wollongong, was liberated from 9-12 mg of dried and thoroughly outgassed whole-rock powders by reaction with ClF_3 at 600°C. Isotopic analyses were performed on a dual-inlet PRISM III mass spectrometer. Linearity and proportionality of the $\delta^{18}O$ scale were maintained by analysing aliquots of three Oztech CO_2 gases with nominal $\delta^{18}O_{VSMOW}$ values of +10.59, +25.04 and +31.22‰, as unknowns, in every analytical session. The data are normalised to NBS-28 quartz ($\delta^{18}O_{VSMOW}$ = +9.64‰; Coplen et al., 1983, Brand et al., 2014). On this scale, by direct analysis against NBS-28, the laboratory quartz working standard (UOW-Q) has a $\delta^{18}O_{VSMOW}$ value of +10.7‰, and is prepared and analysed in each day's batch of ten ClF_3 reactions. All samples were analysed in at least duplicate and the reproducibility of the data (Table 3) is 0.1 to 0.3‰.

6.2. Results

All the felsic schist samples showed extremely elevated $\delta^{18}O_{VSMOW}$ values of +14.6 to +16.2‰ (Fig. 11). These whole rock compositions are not in equilibrium with the $\delta^{18}O$ ~ +5‰ of magmatic zircons found in the same rocks (Hiess et al., 2009). Sample G97/18 of an unaltered ~3800 Ma tonalite south of the Isua supracrustal belt yielded a $\delta^{18}O_{VSMOW}$ value of +7.8‰, likely to be in isotopic equilibrium with magmatic zircon in the same rock with a $\delta^{18}O_{VSMOW}$ value of +5.0‰ (Hiess et al., 2009). Different lithologies in the Isua region display a range of whole rock $\delta^{18}O$ values (Fig. 4), but with strongly positive values never being found in any plutonic rocks and chemically unaltered volcanic rocks (data in Baadsgaard et al., 1986b; Pope et al., 2012).

7. Discussion

7.1. Protolith of the Isua 3806 Ma felsic schists

The Isua 3806 Ma felsic schists show similar La/Yb(N) and REE abundances compared with ~3800 Ma tonalites and granodiorites south of the Isua supracrustal belt (samples G97/18 and G97/98, respectively, in Fig. 9B). However the closest match is found with the REE and other trace-element chemistry of more evolved ancient volcanic rocks, such as non-silicified parts of the Kittys Gap unit of the Palaeoarchaean Warrawoona Group (Fig. 9B; Smithies et al., 2007). Therefore, the magmatic protolith of the felsic schist unit is regarded to contain some more evolved compositions such as rhyolite, rather than solely volcanic equivalents (dacites) of the ~3800 Ma tonalites and granodiorites south of the Isua supracrustal belt.

The potassic schist whole-rock positive initial ε_{Nd} values of $\geq +2$ (data in Hamilton et al., 1983 and Jacobsen and Dymek, 1988) matches the signatures of ~3800 Ma tonalites and mafic rocks in the Isua area (e.g. Bennett et al., 1993, 1997). Likewise, the magmatic zircons of the unit show initial ε_{Hf} values of ~0, indistinguishable from the ~3800 Ma tonalite zircons (Hiess et al., 2009). Therefore, these rocks do not represent the products of recycling of significantly older (>100 million years) or weathered crust. However, it is uncertain whether they were generated by fractional crystallisation of tonalitic magmas or by remelting of juvenile crust, formed within the previous <100 million years.

Unlike modern, non-metamorphosed volcanic rocks, the amphibolite facies metamorphism and the ductile deformation of the Isua felsic schists have obliterated most of the textural and mineralogical evidence of the processes that formed them. However, the intra-zircon magmatic petrology plus a few rare low-strain domains in the rocks indicate that they are clearly *not* derived by metasomatism of tonalites or

mafic rocks (as was proposed by Rosing et al., 1996 and Myers, 2001). Instead, they are interpreted to be of volcanic origin, possibly including some ignimbritic units (e.g. Fig. 3F).

Some of the matrix at the felsic nodule locality (the source of the majority of samples used in this study) is extremely carbonate rich (up to ~12 wt% CO_2). Although some carbonate forms veins with reaction selvedges in silicate rocks and thus clearly formed in superimposed tectonothermal events (e.g., Rosing et al., 1996 - as happens for carbonates in all orogens of all ages), it is still apparent that in places the felsic nodules are disrupted/fractured (boundinaged) layers in a more ductile carbonate-rich matrix (e.g., Fig. 3C and Nutman, 1986 Fig. 10). In which case, we contend that two different carbonatisation events can be recognised, one of which was early and prior to superimposed tectonothermal events with its associated local high temperature metasomatism.

7.2. Rb-Sr isotopic constraints on alteration timing

Rocks from the nodule locality yield a well-defined linear array on an $^{87}Sr/^{86}Sr$ versus $^{87}Rb/^{86}Sr$ diagram, with a large spread in $^{87}Rb/^{86}Sr$ (ranging between 3-25, with the majority of samples >10) and with a slope equivalent to 3760±140 Ma (Jacobsen and Dymek, 1988). In the northern edge of the Isua supracrustal belt, less than 1 km from the nodule locality, there is a deformed internally-fractionated pegmatite sheet, from which 5 samples with $^{87}Rb/^{86}Sr$ ranging between 10 to 448 yielded a $^{87}Sr/^{86}Sr$ versus $^{87}Rb/^{86}Sr$ linear array, with a slope equivalent to 3420±140 Ma, and for that age, the remarkably high initial $^{87}Sr/^{86}Sr$ of 0.811±0.043 (Baadsgaard et al., 1986b). This high initial $^{87}Sr/^{86}Sr$ does not permit derivation of these pegmatites from sources such as regional ~3800 and ~3700 Ma tonalites and ~3650 Ma granites, because the present-day $^{87}Sr/^{86}Sr$ of these rocks is only 0.709 to 0.9049 and would have been too

low at 3420±140 Ma to yield the pegmatite initial compositions. However, as discussed in Baadsgaard et al. (1986) the ~3800 Ma 'nodule' locality rocks with overall higher $^{87}Rb/^{86}Sr$ of 15-20 and present day $^{87}Rb/^{86}Sr$ >1.0 would have had appropriate Sr isotopic compositions to be the source of the pegmatites. This supports the notion that the chemical alteration with Rb-Sr fractionation of the 'nodule' locality volcanic unit is a very early feature, possibly at ~3800 Ma.

7.3. Interpretation of Isua whole-rock oxygen isotopic signatures

Isua area ~3800 Ma rocks show a broad range in $\delta^{18}O_{VSMOW}$ values from +1.5 to +16.2‰ (Fig. 4, Table 3 and data in Baadsgaard et al., 1986 and Pope et al., 2012). All these rocks have fresh Archaean amphibolite facies mineral assemblages (Nutman, 1986) with minimal post last glacial maximum Arctic weathering rinds (~1 mm) developed on the surface. Therefore the range of oxygen isotope signatures is not a result of modern weathering. Most of the metagranitoids in the region show $\delta^{18}O_{VSMOW}$ values between ~+6.0 and +7.5‰, indicating that they retain their igneous signature (Baadsgaard et al., 1986a; Hiess et al., 2009). Exceptions are low $\delta^{18}O_{VSMOW}$ values of <+5 in high-temperatue fluid-dominated shear zones (Baadsgaard et al., 1986a) and anomalously high values in rocks interpreted on other geochemical and field criteria to have undergone ancient weathering (this paper).

Two samples of ~3800 Ma tonalites several kilometres south of the Isua supracrustal belt (samples 225858 and G97/18; Fig. 1) have $\delta^{18}O_{VSMOW}$ values of +6.5 and +7.8‰ respectively (Fig. 4). Magmatic zircons from G97/18 have $\delta^{18}O_{VSMOW}$ = +5.0‰ (Hiess et al., 2009; Fig. 11), meaning that at the zircon crystallisation temperature of ~700°C (Hiess et al., 2008) the zircons and whole rock may be in isotopic equilibrium. Ca. 3800 Ma tonalites 225942, 225943 and 225841 at the southern margin of the Isua supracrustal belt (Fig. 1) have magmatic $\delta^{18}O_{VSMOW}$ values

of +7.3 to +7.5‰ (Fig. 4; Baadsgaard et al., 1986a). Metabasaltic amphibolites in the southern part of the Isua supracrustal belt have $\delta^{18}O_{SMOW}$ values of +5.1 to +7.7‰ (Pope et al., 2012), overlapping expected mantle-derived igneous compositions, but suggestive of a minor, variable ancient weathering signature. Dolomite marbles with seawater-like trace-element signatures (Nutman et al., 2010) that crop out between the aforementioned metabasaltic amphibolites and the 3806 Ma felsic schist unit have $\delta^{18}O_{VSMOW}$ values of +12.3 to +12.5‰ (Fig. 4; Chivas, unpublished data): these oxygen isotopic compositions are expected in Eoarchaean sedimentary carbonates (see data compilation and temporal analysis of Jaffrés et al., 2007). These values are not as elevated as those found in the overlying 3806 Ma felsic schist unit (≥ +14.6‰). In sample 248203 with a whole-rock $\delta^{18}O_{VSMOW}$ value of +16.2‰, the magmatic zircons show mantle-like oxygen of +5.0‰ (Hiess et al., 2009). This demonstrates that the whole-rock and zircon oxygen are not in isotopic equilibrium, and that the igneous protoliths of the felsic schists as recorded by zircon compositions did *not* have elevated $\delta^{18}O_{VSMOW}$ values.

The oxygen isotope data from the Isua area ~3800 Ma rocks shows that suites of ~3800 Ma basaltic and tonalitic rocks formed with mantle-like signatures, but were variably modified afterwards, *prior* to regional metamorphism. We contend that the variation is best explained by variable degrees of weathering and hydrothermal alteration immediately after the ~3800 Ma igneous rocks formed. The basaltic amphibolites have relict pillow structures and show moderate elevation of $\delta^{18}O_{VSMOW}$ up to +7.7‰. On the other hand the 3806 Ma felsic schists preserve possible ignimbritic structures (Fig. 3), hinting that eruption of their protoliths was most likely sub-aerial; an environment where more aggressive weathering with greater modification of the oxygen isotope signature is likely.

Palaeo-Eoarchaean pegmatites along the northern margin of the Isua supracrustal belt including near the nodule locality (samples 225926, 229472 and 229405 on Fig. 1; Baadsgaard et al., 1986a) have elevated $\delta^{18}O_{VSMOW}$ values of +8.7 to +9.2‰. Samples from a related similar pegmatite (see above) have an early Archaean Rb-Sr age with an extremely high initial $^{87}Sr/^{86}Sr$ ratio. Thus these pegmatites were generated from a source where the Sr was already highly radiogenic, but also had elevated $\delta^{18}O_{VSMOW}$. This is further evidence that the event generating the elevated $\delta^{18}O_{VSMOW}$ values of the 3806 Ma felsic schist unit was linked to the loss of Sr, and increase of Rb/Sr and both were imprinted in the Eoarchaean.

7.4. Environment of potassic alteration

The key geochemical alteration features of the felsic schist unit are elevated $\delta^{18}O_{VSMOW}$ values relative to the magmatic compositions represented by zircons (Fig. 11), increase in K/Na via Na loss (Fig. 8A), no enrichment in silica or alumina (Table 2) and increase in Rb/Sr via loss of Sr (Fig. 8B). The elevated $\delta^{18}O_{VSMOW}$ values demonstrate that alteration took place at a low temperature.

The ultimate reason for the alteration is the combination of atmospheric CO_2 and water to produce carbonic acid that reacts with silicate minerals. Note that these hydrolysis reactions are independent of atmospheric oxygen levels, thus can be expected to have operated on the early Earth prior to the early Palaeoproterozoic oxygenation of the atmosphere (Holland et al., 1986; Kasting, 1987). Beyond that low temperatures are dictated by the elevated $\delta^{18}O_{VSMOW}$ values, important controlling factors to derive different hydrolysis alteration mineral assemblages are the water/rock ratio, fluid K^+/Na^+, K^+/H^+ and H_4SiO_4 activity. At lower H_4SiO_4 activity, K^+/Na^+, K^+/H^+ will dictate whether igneous potassic feldspar and plagioclase are converted to adularia, or whether feldspars are converted to clay minerals such as found in kaolinite

development (e.g., Rougvie and Sorensen, 2002; Rouchon and Orberger, 2008). In the case of the Isua felsic schists, superimposed polyphase amphibolite facies metamorphism has recrystallised the original low-temperature assemblages. Nonetheless, in thin sections of the nodules, K-feldspar is abundant, but relict plagioclase phenocrysts are being replaced by muscovite ± alkali feldspar (Fig. 3C, G). This shows that during alteration K-feldspar was stable but that alteration of plagioclase involved replacement by K-feldspar plus formation of some illite (as a precursor to muscovite in the metamorphic assemblage?). Nonetheless, the overall abundance of muscovite in the studied nodule samples is low, suggesting that most alteration of plagioclase gave rise to K-feldspar.

At high activity of H_4SiO_4 (> ~log-2.5) amorphous silica will be the stable phase. In some Archaean felsic volcanic sequences potassic alteration is combined with strong silicification (e.g., Rouchon and Orberger, 2008 and references therein). This combination is ascribed to subaqueous deposition of particulate tuffaceous materials (i.e. a very high water/rock ratio), together with silica precipitation from a low-pH hydrosphere under a high pCO_2 atmosphere (Rouchon and Orberger, 2008). Therefore the lack of silica enrichment suggests that the Isua schists were not in a very high water/rock ratio environment. Some types of weathering result in a strong enrichment of Al_2O_3 via the formation of kaolinite, with the removal of K, Na and Ca in solution. This form of weathering is common in laterites, under a wet and commonly warm climate. Again, the Isua felsic schists do not show these geochemical traits, and hence a wet climate can be discounted. On the other hand, Rougvie and Sorensen (2002) report that the subaerial weathering (i.e., lower rock/water ratio) of Cenozoic Socorro tuffs from the southwestern United States resulted in replacement of igneous alkali and plagioclase feldspars by adularia (± some clays), causing elevated K_2O/Na_2O. In this process there was little modification of SiO_2 and Al_2O_3 because

reactions involved predominantly a simple $Na^+ \leftrightarrow K^+$ ionic exchange in the alkali feldspars and albite and some K-addition for the replacement of the minor anorthite component in plagioclase (Rougvie and Sorensen, 2002). For the Socorro tuffs, the field of Na_2O versus K_2O is congruent with that of the Isua felsic schists (Fig. 8A), and they show similar degrees of increase in $\delta^{18}O_{VSMOW}$. For these tuffs, temperatures of alteration have been estimated at 30-80°C, based on stable isotope signatures and mineral assemblages (Ennis et al., 2000), and the alteration environment is subaerial with low precipitation (Rougvie and Sorensen, 2002). Therefore we contend that potassic alteration of the dacitic and rhyolitic protoliths of the Isua felsic schist unit occurred at ~3800 Ma, at low temperatures and under a subaerial environment with modest precipitation (or at least low percolation rates).

7.5. *Significance of dolomitisation - ~3800 Ma biomediation?*

The Isua felsic schists show a positive correlation between MgO - CaO and MgO - CO_2 (Figs. 8C, D). The vectors on these plots suggest that the mineralogical control was calcic dolomite or stoichiometric dolomite + minor calcite. There is no clear correlation between MgO and W (the weathering factor) on the MFW plot. This indicates that carbonate addition was independent of the degree of potassic alteration. Some carbonate is present in veins, but elsewhere it is pervasive throughout the rocks (e.g. Fig. 2C). Although requiring further confirmation, we contend that precipitation of the dolomite was also a low-temperature phenomenon, perhaps permitted by decreasing acidity of groundwater with waning circulation late in the alteration process (e.g., Rouchon and Orberger, 2008).

Low-temperature dolomite has only been observed to form as a result of anaerobic microbial mediation, and has been documented in modern sediments and groundwater-basalt systems, with several different metabolic pathways and waters of

different composition (Moore et al., 2004; Roberts et al., 2004; Douglas, 2005; Wright and Oren, 2005 and references therein; Wright and Wacey, 2005). These cases of dolomite formation have been replicated under controlled conditions in the laboratory (e.g. Vasconcelos et al., 1995; Roberts et al., 2004; Wright and Wacey, 2004, 2005), making a compelling case that microbial mediation is essential for low-temperature precipitation of dolomite in saline solutions (Douglas, 2005; Wright and Oren, 2005; Wacey et al., 2007). Therefore, we propose that the volcanic protoliths of the Isua 3806 Ma felsic schists might have harboured subterranean 3806 Ma microbial life, whose carbonate production completed the chemical alteration of original rhyolites and dacites.

8. Conclusions

(1) In the ~3806 Ma Isua felsic schists, low strain domains preserve quartz amygdules, small K-feldspar and plagioclase phenocrysts in a very fine-grained matrix with possible local fiamme texture, and show that the protoliths of the felsic schist unit were felsic volcanic rocks, not altered tonalites or mafic rocks as suggested by some other researchers.

(2) Zircons from both nodules and more carbonate-rich matrix are magmatic in origin, and contain axial lobate voids indicating crystallisation at high crustal levels or during eruption. Such features are never observed in the igneous zircons of deep plutonic granitoids. The zircons contain quartz + rutile inclusions, and yield Ti-in-zircon temperatures of 750-650°C. Combined with the presence of the fluid voids in the zircons and amygdules in the whole rocks, this indicates low temperature crystallisation of a hydrous magma.

(3) Key isotopic deviations from unaltered igneous compositions are indicated by the disequilibrium between $\delta^{18}O_{VSMOW}$ of zircon (~ +5‰) and whole rocks (up to +15‰),

high K_2O/Na_2O due to low Na_2O, high Rb/Sr due to low Sr, yet no radical change in SiO_2 and Al_2O_3 contents. These features are best explained by low-temperature alteration (such as weathering) via feldspar cation exchange with percolating fluids, leading to replacement of alkali feldspar by K-feldspar and the degradation of plagioclase with its replacement by K-feldspar ± clays.

(4) The geochemical variation of samples not affected by dolomitisation suggests that the protoliths of the schists included both dacitic and rhyolitic compositions.

(5) This is the oldest-known low-temperature alteration, and shows that almost 4 billion years ago there was drawdown of atmospheric CO_2, that combined with water caused low temperature alteration of feldspars. This is similar to processes observed throughout the geological record.

(6) An additional process in the felsic schist unit is variable degrees of early (pre-tectonic) dolomitisation. On the caveat that this is also a low-temperature process, and that low-temperature dolomitisation is only known to occur by biomediation, this would show that the porous, altered felsic volcanic unit harboured 3806 Ma subterranean life.

Acknowledgements

This project is supported by ARC project DP120100273 and the GeoQuEST Research Centre of the University of Wollongong. The Geological Survey of Denmark and Greenland is thanked for permission to publish this paper, which includes the 1970s geochemical data on survey samples and uses the sample 248202 and 248203 zircons for further study. David Wheeler is thanked for technical assistance with whole rock oxygen isotope analysis. Ole Christiansen of Nunaminerals A/S is thanked for field logistical support.

References

Allaart, J.H., 1976. The pre-3760 m.y. old supracrustal rocks of the Isua area, central West Greenland, and the associated occurrence of quartz-banded ironstone. In: B.F. Windley (Editor), The Early History of the Earth. Wiley, London, pp. 177-189.

Appel, P.W.U., Polat, A., Frei, R., 2009. Dacitic ocelli in mafic lavas, 3.8–3.7 Ga Isua greenstone belt, West Greenland: Geochemical evidence for partial melting of oceanic crust and magma mixing. Chemical Geology 258, 105-124

Baadsgaard, H., Nutman, A.P., Bridgwater, D., McGregor, V.R., Rosing, M., Allaart, J.H., 1984. The zircon geochronology of the Akilia association and the Isua supracrustal belt, West Greenland. Earth Planetary Science Letters 68, 221-228.

Baadsgaard, H., Nutman, A.P., Rosing, M., Bridgwater, D., Longstaffe, F.J., 1986a. Alteration and metamorphism of Amîtsoq gneisses from the Isukasia area, West Greenland: Recommendation for isotope studies of the early crust. Geochimica et Cosmochimica Acta 50, 2165-2172.

Baadsgaard, H., Nutman, A.P., Bridgwater, D., 1986b. Geochronology and isotopic variation of the early Archaean Amîtsoq gneisses of the Isukasia area, southern West Greenland. Geochimica Cosmochimica Acta 50, 2173- 2183.

Bennett, V.C., Nutman, A.P., McCulloch, M.T., 1993. Nd isotopic evidence for transient, highly depleted mantle reservoirs in the early history of the Earth. Earth and Planetary Science Letters 119, 299-317.

Bennett, V.C., Brandon, A., Nutman, A.P., 2007. Coupled ^{142}Nd-^{143}Nd isotopic evidence for Hadean mantle dynamics. Science 318, 1907-1910.

Bolhar, R., Kamber, B.S., Moorbath, S., Fedo, C.M., Whitehouse, M.J., 2004. Characterisation of early Archaean chemical sediments by trace element signatures. Earth Planetary Science Letters 222, 43–60.

Bohlar, R., Kamber, B.S., Moorbath, S., Whitehouse, M.J., Collerson, K.D., 2005. Chemical characterization of earth's most ancient clastic metasediments from the Isua Greenstone Belt, southern West Greenland. Geochimica et Cosmochimica Acta, 69, 1553-1573.

Bowring, S.A., Williams, I.S., 1999. Priscoan (4.00-4.03) orthogneisses from northwestern Canada. Contributions Mineralogy Petrology 134, 3-16

Bowring, S.A., Williams, I.S., Compston, W., 1989. 3.96 Ga gneisses from the Slave province, Northwest Territories, Canada. Geology 17, 760-764.

Brand, W.A., Coplen, T.B., Vogl, J., Rosner, M., Prohaska, T., 2014. Assessment of international reference materials for isotope-ratio analysis (IUPAC Technical Report). Pure and Applied Chemistry 86, 425-467.

Compston, W., Kinny, P.D., Williams, I.S., Foster, J.J., 1986. The age and lead loss behaviour of zircons from the Isua supracrustal belt as determined by ion microprobe. Earth and Planetary Science Letters 80, 71-81.

Coplen, T.B., Kendall, C., Hopple, J., 1983. Comparison of stable isotope reference samples. Nature 302, 236-238.

Crowley, J.L., 2003. U-Pb geochronology of 3810-3630 Ma granitoid rocks south of the Isua greenstone belt, southern West Greenland. Precambrian Research 126, 235-257.

Crowley, J.L., Myers, J.S., Dunning, G.R., 2002. Timing and nature of multiple 3700-3600 Ma tectonic events in intrusive rocks north of the Isua greenstone belt, southern West Greenland. Geological Society of America Bulletin 114, 1311-1325.

Douglas, S., 2005. Mineralogical footprints of microbial life. American Journal of Science 305, 503-525.

Dymek, R.F. and Klien, C., 1988. Chemistry, petrology and origin of banded iron-formation lithologies from the 3800 Ma Isua supracrustal belt, west Greenland. Precambrian Research 39, 247-302.

Dymek, R.F., Brothers S.C., Schiffries, C. M., 1988. Petrogenesis of ultramafic metamorphic rocks from the 3800 Ma Isua supracrustal belt, West Greenland. Journal of Petrology 29, 1353-1397.

Ennis, D.J., Dunbar, N.W., Campbell, A.R., Chapin, C.E., 2000. The effects of K-metasomatism on the mineralogy and geochemistry of silicic ignimbrites near Socorro, New Mexico. Chemical Geology 167, 285-312.

Fedo, C.M., 2000. Setting and origin of problematic rocks from the >3.7 Ga Isua greenstone belt, southern West Greenland: Earth's oldest coarse clastic sediments. Precambrian Research 101, 69-78.

Ferry, J. M. and Watson, E. B. 2007. New thermodynamic models and revised calibrations for the Ti-in-zircon and Zr-in-rutile thermometers. Contributions to Mineralogy and Petrology 154, 429-437.

Friend, C.R.L., Nutman, A.P., 2011. Dunites from Isua, Greenland: A ca. 3720 Ma window into subcrustal metasomatism of depleted mantle. Geology 39, 663-669.

Friend, C.R.L., Bennett, V.C., Nutman, A.P., Norman, M.D. 2007. Seawater-like trace element signatures (REE + Y) of Eoarchaean chemical sedimentary rocks from southern West Greenland, and their corruption during high-grade metamorphism. Contributions Mineralogy and Petrology 155, 229-246.

Furnes, H., de Wit, M., Staudigel, H., Rosing, M., Muehlenbachs, K., 2007. Vestige of Earth's oldest ophiolite. Science 215, 1704-1707.

Gill, R.C.O., 2011. Igneous rocks and processes, a practical guide. Wiley-Blackwell, 428 pp.

Hamilton, P.J., O'Nions, R.K., Evensen, N.H., Bridgwater, D., Allaart, J.H., 1978. Sm-Nd isotopic investigations of Isua supracrustals and implications for mantle evolution. Nature 272, 41-43.

Hiess, J., Bennett, V. C., Nutman, A. P., and Williams, I. S., 2009. In situ U–Pb, O and Hf isotopic compositions of zircon and olivine from Eoarchaean rocks, West Greenland: New insights to making old crust. Geochimica et Cosmochimica Acta 73, 4489–4516.

Hoffmann, J. E., Münker, C., Naeraa, T., Rosing, M. T., Garbe-Schönberg D., Svahnberg, H., 2011. Mecahisms of Archean crust production inferred from high precision HFS systematics in TTGs: Geochimica et Cosmochimica Acta **7**5, 4175-4178.

Holland, H.D., Lazar, B., McCaffrey,M., 1986. Evolution of the atmosphere and oceans. Nature 320, 27–33.

Hoskin, P.W.O., 2005. Trace-element composition of hydrothermal zircon and the alteration of Hadean zircon from the Jack Hills, Australia. Geochimica et Cosmochimica Acta 69, 637-648.

Jacobsen, S.B., Dymek, R.F., 1988. Nd and Sr isotope systematics of clastic metasediments from Isua, West Greenland: Identification of pre-3.8 Ga differentiated crustal components. Journal of Geophysical Research 93, 338-354.

Jaffrés, J.B.D., Shields, G.A., Wallman, K., 2007. The oxygen isotope evolution of seawater: A critical review of a long-standing controversy and an improved geological water cycle model for the past 3.4 billion years. Earth Sciences Reviews 83, 83-122.

Jenner, F.E., Bennett, V.C., Nutman, A.P., Friend, C.R.L., Norman, M.D., Yaxley, G. 2009. Evidence for subduction at 3.8 Ga: Geochemistry of arc-like metabasalts from the southern edge of the Isua Supracrustal Belt. Chemical Geology 261, 83-98.

Kasting, J.F., 1987. Theoretical constraints on oxygen and carbon-dioxide concentrations in the Precambrian Atmosphere. Precambrian Research 34, 205–229.

Komiya, T., Maruyama, S., Masuda, T, Appel., P.W.U., Nohda, S., 1999. The 3.8-3.7 Ga plate tectonics on the Earth; Field evidence from the Isua accretionary complex, West Greenland. Journal Geology 107, 515-554.

Le Maitre, R.W., Streikeisen, A., Zanettin, B., Le Bas. M.J.,Bonin, B., Bateman, P., Bellieni, G., Dudek, A., Efremova, S., Keller, J., Lameyre, J., Sabine, P.A., Schmid, R., Sorensen, H., Wolley, A.R., 2005. Igneous rocks – a classification and glossary of terms. Recommendations of the IUGS subcommision on the systematics of igneous rocks. Cambridge, Cambridge University Press. 2nd edition, 256 pp.

Martin, H., 1994. The Archean grey gneiss and the genesis of continental crust. In: Condie, K.C. (Ed.), Archean Crustal Evolution. Elsevier, Amsterdam, 205-259.

McDonough, W.F., Sun, S.S., 1995. The composition of the Earth. Chemical Geology 120, 223–253.

Michard-Vitrac, A., Lancelot, J. Allegre, C.J., Moorbath, S., 1977. U-Pb ages on single zircons from early Precambrian rocks of West Greenland and the Minnesota River Valley. Earth and Planetary Sciences Letters 35, 449-453.

Moore, T.S., Murray, R.W., Kurtz, A.C., Schrag, D.P., 2004. Anaerobic methane oxidation and the formation of dolomite. Earth and Planetary Science Letters 229, 141-154.

Myers, J.S., 2001. Protoliths of the 3.8–3.7 Ga Isua greenstone belt, West Greenland. Precambrian Research 105, 129-141.

Nutman, A.P., 1986. The geology of the Isukasia region, southern West Greenland. Grønlands geologiske Undersøgelse Bulletin 154, 80 pp.

Nutman, A.P., Bridgwater, D., 1986. Early Archaean Amîtsoq tonalites and granites from the Isukasia area, southern West Greenland: Development of the oldest-known sial. Contributions to Mineralogy and Petrology 94, 137-148.

Nutman, A.P., Friend, C.R.L., 2009. New 1:20000 geological maps, synthesis and history of the Isua supracrustal belt and adjacent gneisses, Nuuk region, southern West Greenland: A glimpse of Eoarchaean crust formation and orogeny. Precambrian Research 172, 189-211.

Nutman, A.P., Bridgwater, D., Dimroth, E., Gill, R.C.O., Rosing, M., 1983. Early (3700 Ma) Archaean rocks of the Isua supracrustal belt and adjacent gneisses. Rapport Grønlands geologiske Undersøgelse, 112, 5-22.

Nutman, A.P., Allaart, J.H., Bridgwater, D. Dimroth, E., Rosing, M.T., 1984. Stratigraphic and geochemical evidence for the depositional environment of the early Archaean Isua supracrustal belt, southern West Greenland. Precambrian Research 25, 365-396.

Nutman, A.P., Friend, C.R.L., Kinny, P.D., McGregor, V.R., 1993. Anatomy of an Early Archaean gneiss complex: 3900 to 3600 Ma crustal evolution in southern West Greenland. Geology 21, 415-418.

Nutman, A.P., McGregor, V.R., Friend, C.R.L., Bennett, V.C., Kinny, P.D., 1996. The Itsaq Gneiss Complex of southern West Greenland; the world's most extensive record of early crustal evolution (3900-3600 Ma). Precambrian Research 78, 1-39.

Nutman, A.P., Bennett, V.C., Friend, C.R.L., Rosing, M.T., 1997. ~3710 and ≥3790 Ma volcanic sequences in the Isua (Greenland) supracrustal belt; structural and Nd isotope implications. Chemical Geology 141, 271-287.

Nutman, A.P., Bennett, V.C., Friend, C.R.L., Norman, M.D., 1999. Meta-igneous (non-gneissic) tonalites and quartz-diorites from an extensive ca. 3800 Ma

terrain south of the Isua supracrustal belt, southern West Greenland: Constraints on early crust formation. Contributions Mineralogy Petrology 137, 364-388.

Nutman, A.P., Friend, C.R.L., Bennett, V.C., McGregor, V.R., 2000. The early Archaean Itsaq Gneiss Complex of southern West Greenland: The importance of field observations in interpreting dates and isotopic data constraining early terrestrial evolution. Geochimica et Cosmochimica Acta 64, 3035-3060.

Nutman, A.P., Friend, C.R.L., Bennett, V.C., 2002. Evidence for 3650-3600 Ma assembly of the northern end of the Itsaq Gneiss Complex, Greenland: Implication for early Archean tectonics. Tectonics 21, article 5

Nutman, A.P., Friend, C.R.L. & Bennett, V. 2004. Dating of the Ameralik dyke swarms of the Nuuk district, southern West Greenland: Mafic intrusion events starting from c. 3510 Ma. Journal of the Geological Society, London, 161, 421-430.

Nutman, A.P., Friend, C.R.L., Horie, H., Hidaka, H., 2007. Construction of pre-3600 Ma crust at convergent plate boundaries, exemplified by the Itsaq Gneiss Complex of southern West Greenland. *In:* van Kranendonk, M.J., Smithies, R.H., & Bennett, V.C. (eds) *Earth's Oldest Rocks*. Elsevier, pp.187-218.

Nutman, A.P., Friend, C.R.L., Paxton, S., 2009. Detrital zircon sedimentary provenance ages for the Eoarchaean Isua supracrustal belt, southern West Greenland: Juxtaposition of an imbricated ca. 3700 Ma juvenile arc assemblage against an older complex with 3920-3800 Ma components. Precambrian Research 172, 212-233.

Nutman, A.P., Friend, C.R.L., Bennett, V.C., Wright, D., Norman, M.D., 2010. ≥3700 Ma pre-metamorphic dolomite formed by microbial mediation in the Isua supracrustal belt (W. Greenland): Simple evidence for early life? Precambrian Research 183, 725-737.

Nutman, A.P., Bennett, V.C., Friend, C.R.L., Hidaka, H., Yi, K., Lee, S.R., Kamiichi, T., 2013. The Itsaq Gneiss Complex of Greenland: Episodic 3900 to 3660 Ma juvenile crust formation and recycling in the 3660 to 3600 Ma Isukasian orogeny. American Journal of Science 313, 877-911.

Ohata, T., Arai, H., 2007. Statistical empirical index to chemical weathering in igneous rocks: A new tool for evaluating the degree of weathering. Chemical Geology 240, 280-297.

O'Nions, R.K., Pankhurst, R.J., 1974. Rare earth element distribution in Archaean gneisses and anorthosites, Godthåb area, West Greenland. Earth and Planetary Science Letters 22, 328-338.

Pearce, J.A., Harris, N.B.W., Tindle, A.G., 1984. Trace element discrimination diagrams for the tectonic interpretation of granitic rocks. Journal of Petrology 25, 956-983.

Polat, A., Hofmann, A.W., 2003. Alteration and geochemical patterns in the 3.7-3.8 Ga Isua greenstone belt, West Greenland. Precambrian Research 126, 197-218.

Polat, A., Hofmann, A.W., Rosing, M.T. 2002. Boninite-like volcanic rocks in the 3.7-3.8 Ga Isua greenstone belt, West Greenland: geochemical evidence for intra-oceanic subduction zone processes in the early Earth. Chemical Geology 184, 231-254.

Polat, A., Longstaffe, F., Weisener, C., Fryer, B., Frei, R., Kerrich, R., 2012. Extreme element mobility during transformation of Neoarchean (ca. 2.7 Ga) pillow basalts to a Paleoproterozoic (ca. 1.9 Ga) paleosol, Schreiber Beach, Ontario, Canada. Chemical Geology 326-327, 145-173.

Pope, E.C., Bird, D.K., Rosing, M.T., 2012. Isotope composition and volume of Earth's early oceans. Proceedings of the National Academy of Science doi/10.1073/pnas.1115705109.

Rasmussen, B., Fletcher, I.R., Muhling, J.R., Gregory, C.J., Wilde, S.A., 2011. Metamorphic replacement of mineral inclusions in detrital zircon from Jack Hills, Australia: Implications for the Hadean Earth. Geology, 39, 1143-1146.

Roberts, J.A., Bennett, P.C., González, L.A., Macpherson, G.L., Milliken, K.L., 2004. Microbial precipitation of dolomite in methanogenic groundwater. Geology 32, 277-280.

Roddy, M.S., Reynolds, S.J., Smith, B.M., Ruiz, J., 1988. K-metasomatism and detachment-related mineralization, Harcuvar Mountains, Arizona. Geological Society of America Bulletin 100, 1627-1639.

Rouchon, V., Orberger, B., 2008. Origin and mechanisms of K-Si metasomatism of ca. 3.4-3.3 Ga volcaniclastic deposits and implications for Archean seawater evolution: Examples from cherts of Kittys Gap (Pilbara craton, Australia) and Msauli (Barberton Greenlstone Belt, South Africa). Precambrian Research, 165, 169-189.

Rougvie, J.R., Sorensen, S.S., 2002. Cathodoluminescence record of K-metasomatism in ash-flow tuffs: Grain-scale mechanisms and large scale geochemical implications. Geology 30, 307-310.

Rosing, M.T, Rose, N.M., Bridgwater, D., Thomsen, H.S., 1996. Earliest part of the Earth's stratigraphic record: A reappraisal of the >3.7 Ga Isua (Greenland) supracrustal sequence. Geology 24, 43-46.

Solvang, M., 1999. An investigation of metavolcanic rocks from the eastern part of the Isua greenstone belt, West Greenland. Geological Survey of Denmark and Greenland (GEUS) Internal Report, Copenhagen, Denmark, 62 pages.

Smithies, R.H., Champion, D.C., Van Kranendonk, M.J., 2007. The oldest well-preserved felsic volcanic rocks on Earth: Geochemical clues to the early evolution of the Pilbara Supergroup and implications for the growth of a

Paleoarchean protocontinent. *In:* van Kranendonk, M.J., Smithies, R.H., & Bennett, V.C. (eds) *Earth's Oldest Rocks*. Elsevier, pp.339-367.

Wacey, D., Wright, D. T., Boyce, A. J. 2007. A stable isotope study of microbial dolomite formation in the Coorong Region, South Australia. Chemical Geology 244, 155-174.

Wark, D.A., Hildreth, W., Spear, F.S., Cherniak, D.J., Watson, E.B., 2007. Pre-eruption recharge of the Bishop magma system. Geology 35, 235-238.

Watson, E. B. and Harrison, T. M. 2005. Zircon thermometer reveals minimum melting conditions on earliest Earth. Science 308, 841-844.

Wright, D. T., Oren, A., 2005. Non-photosynthetic bacteria and the formation of carbonates and evaporites through time. Geomicrobiology Journal 22, 27-53.

Wright, D.T., Wacey, D., 2005. Precipitation of dolomite using sulphate-reducing bacteria from the Coorong Region, South Australia: significance and implications. Sedimentology 52, 987-1008.

Vasconcelos, C., McKenzie, J.A., Bernasconi, S., Grujic, D., Tien, A.J., 1995. Microbial mediation as a possible mechanism for natural dolomite at low temperatures. Nature 377, 220-222.

Yuan, H.L., Gao, S., Dai, M.N., Zong, C.L., Günther, D., Fontaine, G.H., Liu, X.M., Diwu, C.R., 2008. Simultaneous determinations of U–Pb age, Hf isotopes and trace element compositions of zircon by excimer laser-ablation quadrupole and multiple-collector ICP-MS. Chemical Geology 247, 100-118.

Table captions

Table 1. Laser Ablation ICP-MS trace element analyses of zircons.

Table 2. Whole rock analyses of the felsic schist unit undertaken in this millennium. See online supplementary Table 1 for full compendium of analyses (1970s to 2010s).

Table 3. Whole rock oxygen isotope data; (a), data in this paper and (b), data from Baadsgaard et al. (1986a). See Figure 1 (map) for localities.

Figure captions

Figure 1. Geological sketch map of the Isua supracrustal belt, based on compilation presented by Nutman and Friend (2009). Discussed localities in the ~ 3800 Ma felsic schist unit are indicated.

Figure 2. (A) Typical quartzo-feldspathic rock within the ~3800 Ma felsic schist unit (65°09.73'N 49°48.90'W). The uniform layering is not a sedimentary/volcanic structure, but is a result of transposition in very strong Eoarchaean deformation. (B) prolate felsic nodules (carbonate-free) in a more strongly-weathering carbonate-bearing matrix (65°05.76'N 50°00.39'W). The nodular-form is a response to ductility contrast during deformation. Location of sample G11/76 is shown. (C) Trains of non-carbonated felsic nodules within strongly carbonated matrix. (D) Low strain domain in the A6 felsic schist unit at the eastern end of the belt (65°09.67'N 49°48.86'W). Layered aphinitic components are disrupted by a felsic fine-grained matrix. This is the location of sample G11/46.

Figure 3. (A) Very fine-grained character of nodule. Note the lenticular pattern, that could be either volcanic or a result of fine-scale fissuring. (Sample G11/76; plane polarised light.). (B) ~0.5 mm K-feldspar grain interpreted as a phenocryst, in a very fine-grained matrix of quartz + feldspar + minor muscovite. (Sample G11/76; cross polarised light.). (C) Relict ~0.5 mm plagioclase phenocryst showing alteration to alkali feldspar ± muscovite. (Sample G11/76; cross polarised light.). (D) Ovoid recrystallised quartz (qtz) interpreted as a weakly deformed amygdule. (Sample G11/76, plane polarised light.). (E) Deformed corroded quartz phenocryst associated with a K-feldspar (ksp) phenocryst set in a fine-grained quartzo-feldspathic groundmass (sample G11/76, cross polarised light.). (F) Structures remembling fiamme in a nodule of the felsic schist unit. Note also the weakly deformed quartz amydules or phenocrysts (qtz). Photograph is reproduced from Nutman et al. (1983), because the whereabouts of the source thin section from the collection of the late D. Bridgwater is unknown. (G) biotite-rich aggregate (clast?) and altered plagioclase phenocryst (altered plag) set in a fine grained matrix. The obtuse angle between the elongation direction of the clast and phenocrysts indicates locally low strain.

Figure 4. Schematic section portraying the pre-deformational relationships between the felsic schist unit and adjacent lithologies.

Figure 5. Petrography of selected zircons. Ringed sites are the location of laser ablation-ICP-MS analyses, with the numerals referring to analyses in Table 1. (A-F) Cathodoluminescence images showing inclusion suites and the presence of axial voids in some zircons. Note coexistence of quartz + rutile, presence of alkali feldspar, but no detection of plagioclase. (G and H) Transmitted and reflected light images of a zircon with an axial void still below the level of the mount’s surface. (I) Transmitted light

image of a zircon containing a transverse acicular apatite inclusion. SEM backscatter imaging (inset) shows that only relict apatite remains. (J) Transmitted light image of a zircon with a polyphase muscovite + galena inclusion (inset SEM backscatter image). The inclusion that has an apatite habit is connected to the grain exterior by a microfracture.

Figure 6. Chondrite-normalised REE plots of zircons from Isua felsic schist samples (A) 248203 nodule and (B) 248202 matrix. (C) Chondrite-normalised REE plot of felsic schist whole-rock samples. Normalising values are from McDonough and Sun (1995).

Figure 7. Ti-in-zircon temperatures for sample 248203 and 248202 zircons. Calculated with the calibration of Ferry and Watson (2007), assuming $aTiO_2$=1.0, because quartz + rutile are found coexisting as inclusions within the zircons (Fig. 3B). Sites with very high Ti attributed to contamination by rutile and/or biotite micro-inclusions have been omitted.

Figure 8. (A) Strong K_2O enrichment and Na_2O depletion, contrary to unaltered Eoarchaean granites and tonalites. Field for Socorro Tuff is from Rougvie and Sorensen (2002). (B) Sr versus Rb plot. (C) CO_2 versus MgO (wt%) plot. (D) CaO versus MgO (wt%) plot. Data for unaltered Eoarchaean tonalites and granites are from Nutman and Bridgwater (1986) and Nutman et al. (1994, 1999). (E) Nb versus Y discrimination diagram. Fields are from Pearce et al. (1984). (F) La/Yb versus Yb (ppm) plot. Fields are from Martin (1994).

Figure 9. Primitive mantle-normalised plots of (A) Isua felsic schist unit rocks and (B) shown compared with ~3800 Ma tonalites and quartz diorites (Nutman et al., 1999) and a non-silicified ~3.46 Ga Kittys Gap volcanic rock from the Pilbara craton (Smithies et al., 2007). Normalising values are from McDonough and Sun (1995).

Figure 10. M (mafic) – F (felsic) – W (weathering) diagram of Ohata and Arai (2007).

Figure 11. $\delta^{18}O_{VSMOW}$ data for zircons (Hiess et al., 2009) and whole-rocks (data presented in this paper and by Baadsgaard et al., 1986a).

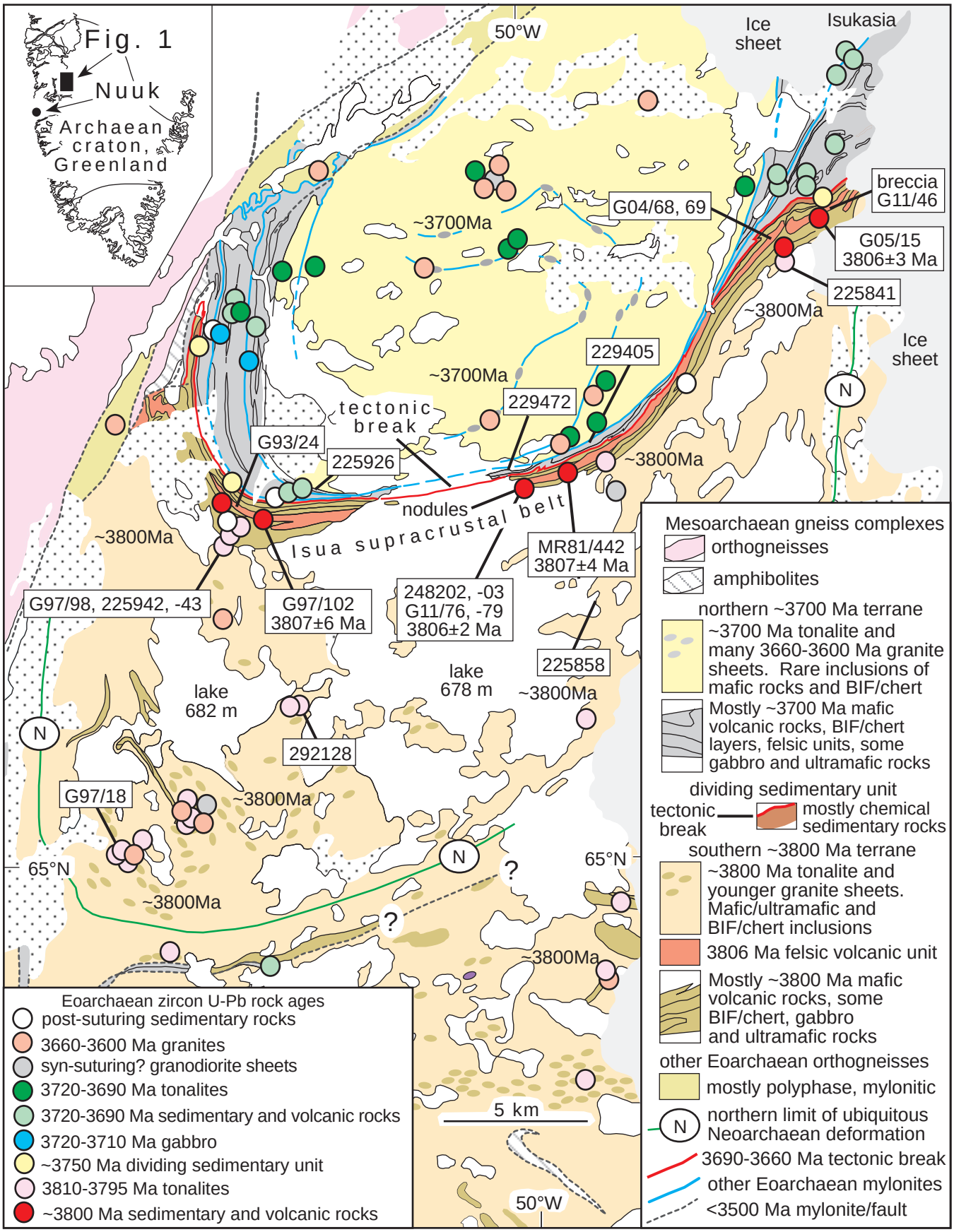
Fig. 1
Nuuk
Archaean craton, Greenland
50°W
Ice sheet
Isukasia
breccia G11/46
G04/68, 69
~3700Ma
G05/15 3806±3 Ma
225841
~3800Ma
Ice sheet
229405
~3700Ma
229472
tectonic break
G93/24
225926
~3800Ma
nodules
Isua supracrustal belt
~3800Ma
MR81/442 3807±4 Ma
G97/98, 225942, -43
G97/102 3807±6 Ma
248202, -03 G11/76, -79 3806±2 Ma
225858
lake 682 m
lake 678 m
~3800Ma
292128
G97/18
~3800Ma
65°N
~3800Ma
65°N
~3800Ma
5 km
50°W
Eoarchaean zircon U-Pb rock ages
post-suturing sedimentary rocks
3660-3600 Ma granites
syn-suturing? granodiorite sheets
3720-3690 Ma tonalites
3720-3690 Ma sedimentary and volcanic rocks
3720-3710 Ma gabbro
~3750 Ma dividing sedimentary unit
3810-3795 Ma tonalites
~3800 Ma sedimentary and volcanic rocks
Mesoarchaean gneiss complexes
orthogneisses
amphibolites
northern ~3700 Ma terrane
~3700 Ma tonalite and many 3660-3600 Ma granite sheets. Rare inclusions of mafic rocks and BIF/chert
Mostly ~3700 Ma mafic volcanic rocks, BIF/chert layers, felsic units, some gabbro and ultramafic rocks
dividing sedimentary unit
tectonic break
mostly chemical sedimentary rocks
southern ~3800 Ma terrane
~3800 Ma tonalite and younger granite sheets. Mafic/ultramafic and BIF/chert inclusions
3806 Ma felsic volcanic unit
Mostly ~3800 Ma mafic volcanic rocks, some BIF/chert, gabbro and ultramafic rocks
other Eoarchaean orthogneisses
mostly polyphase, mylonitic
northern limit of ubiquitous Neoarchaean deformation
3690-3660 Ma tectonic break
other Eoarchaean mylonites
<3500 Ma mylonite/fault

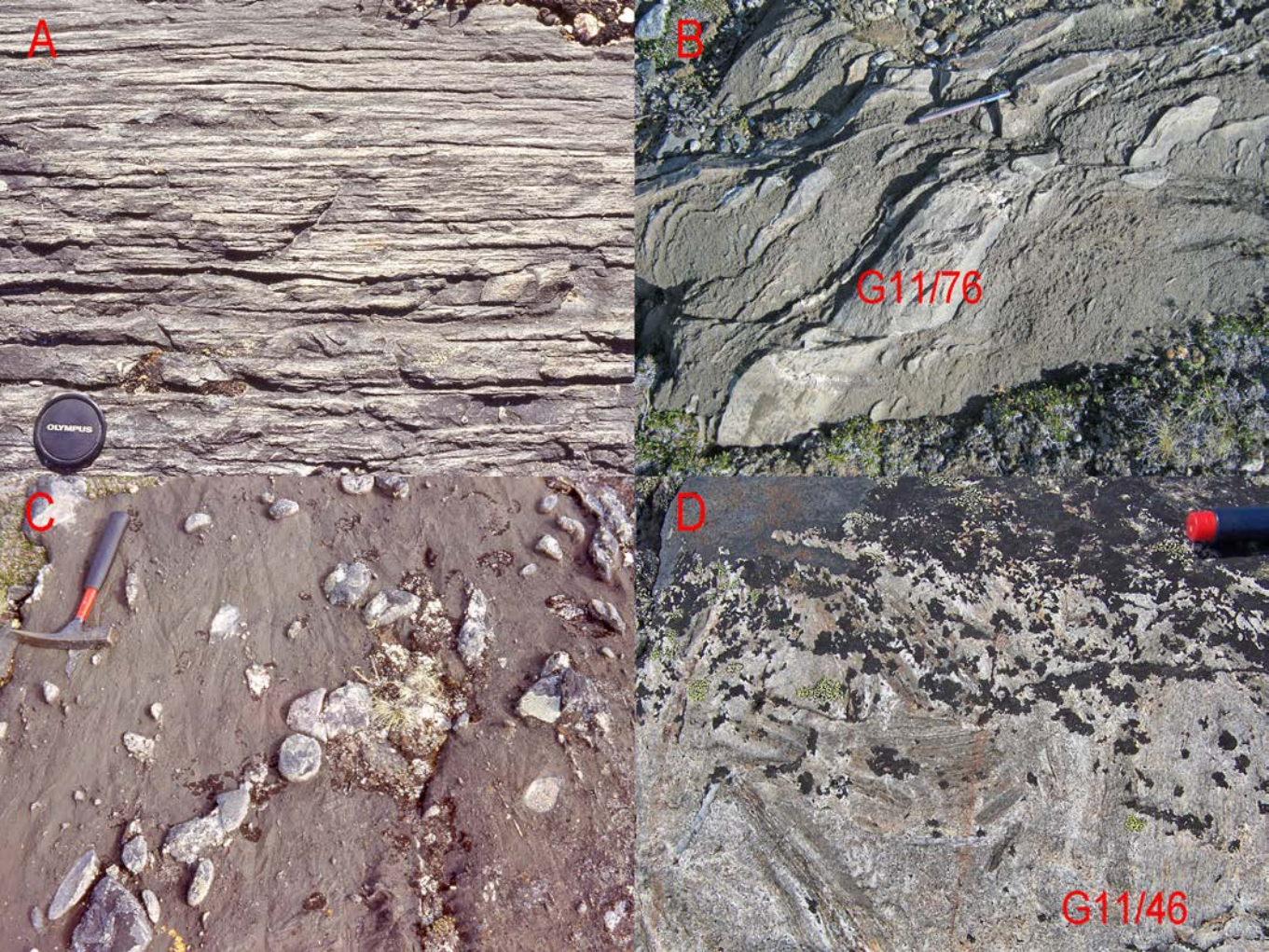
A
OLYMPUS
B
G11/76
C
D
G11/46

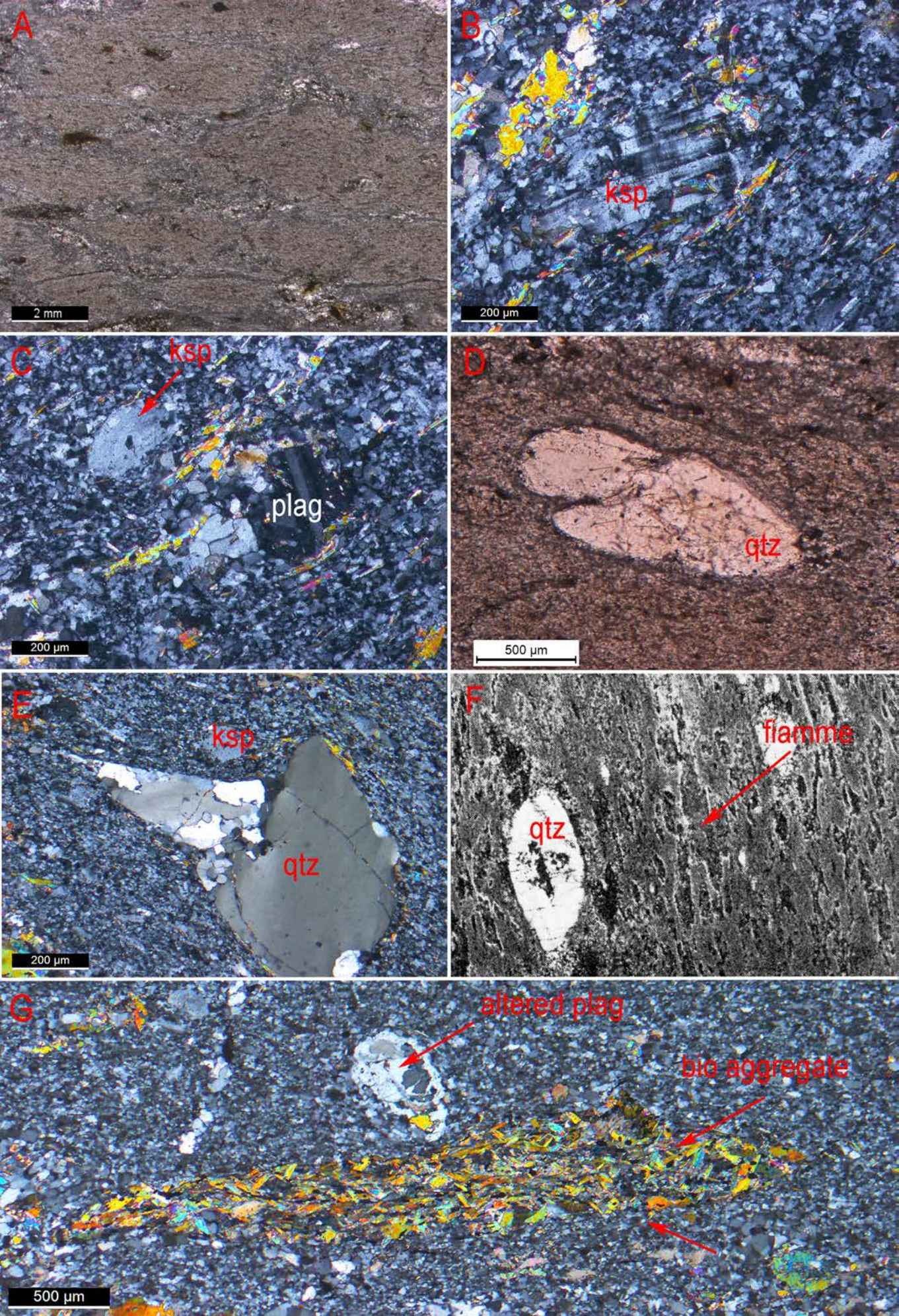
A
2 mm
B
ksp
200 µm
C
ksp
plag
200 µm
D
qtz
500 µm
E
ksp
qtz
200 µm
F
fiamme
qtz
G
altered plag
bio aggregate
500 µm

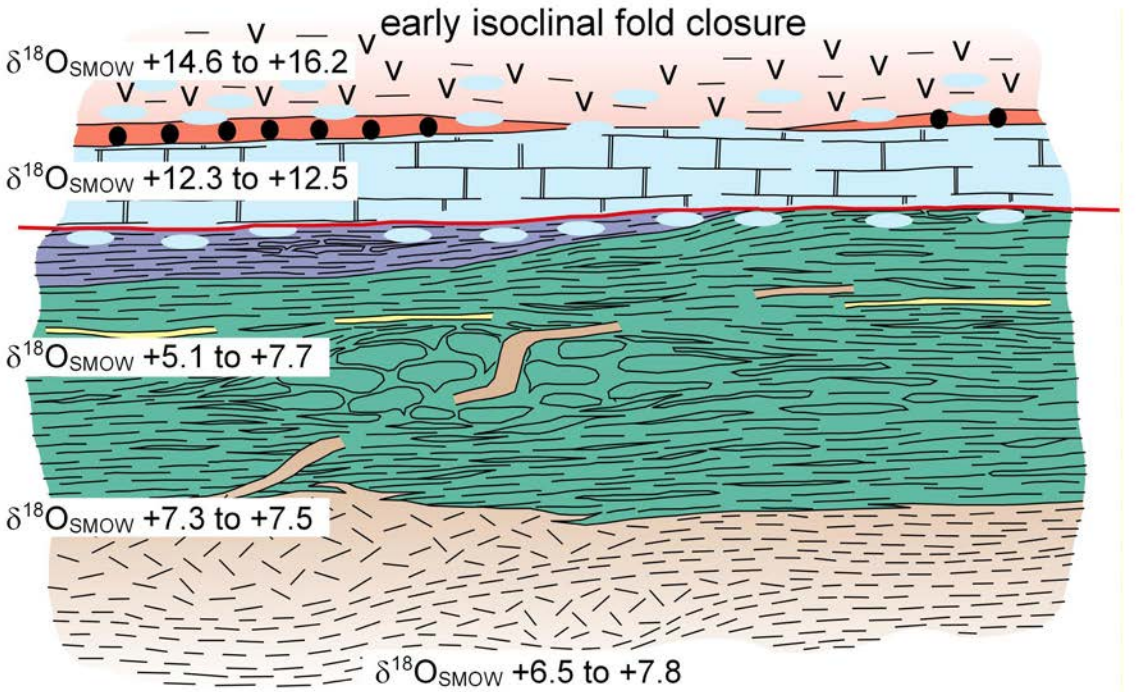

3800-3795 Ma tonalite

3806 Ma felsic schist unit

fuchsitic quartzite with 3890-3810 Ma detrital zircons

dolomitic marble + calc-silicate and siliceous rocks

tectonised boundary, probably modified unconformity

>3800-3795 Ma picrite

siliceous layers (cherts?) in >3800-3795 Ma basalts

>3800-3795 Ma basalts with relict pillow structure

strongly deformed >3800-3795 Ma basalts

carbonate alteration

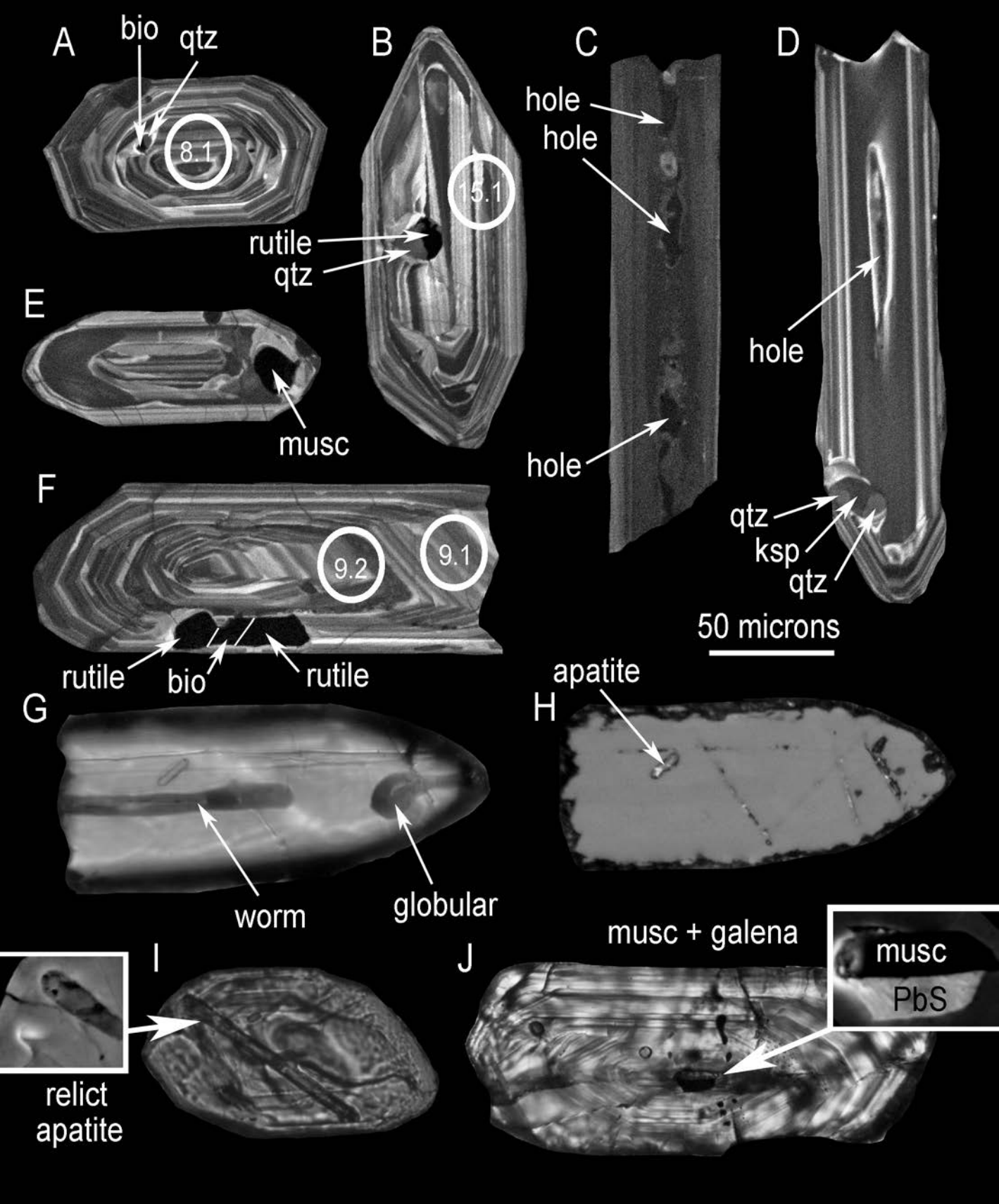
A
bio
qtz
8.1
B
15.1
rutile
qtz
C
hole
hole
hole
D
hole
qtz
ksp
qtz
50 microns
E
musc
F
9.2
9.1
rutile
bio
rutile
G
worm
globular
H
apatite
I
relict
apatite
J
musc + galena
musc
PbS

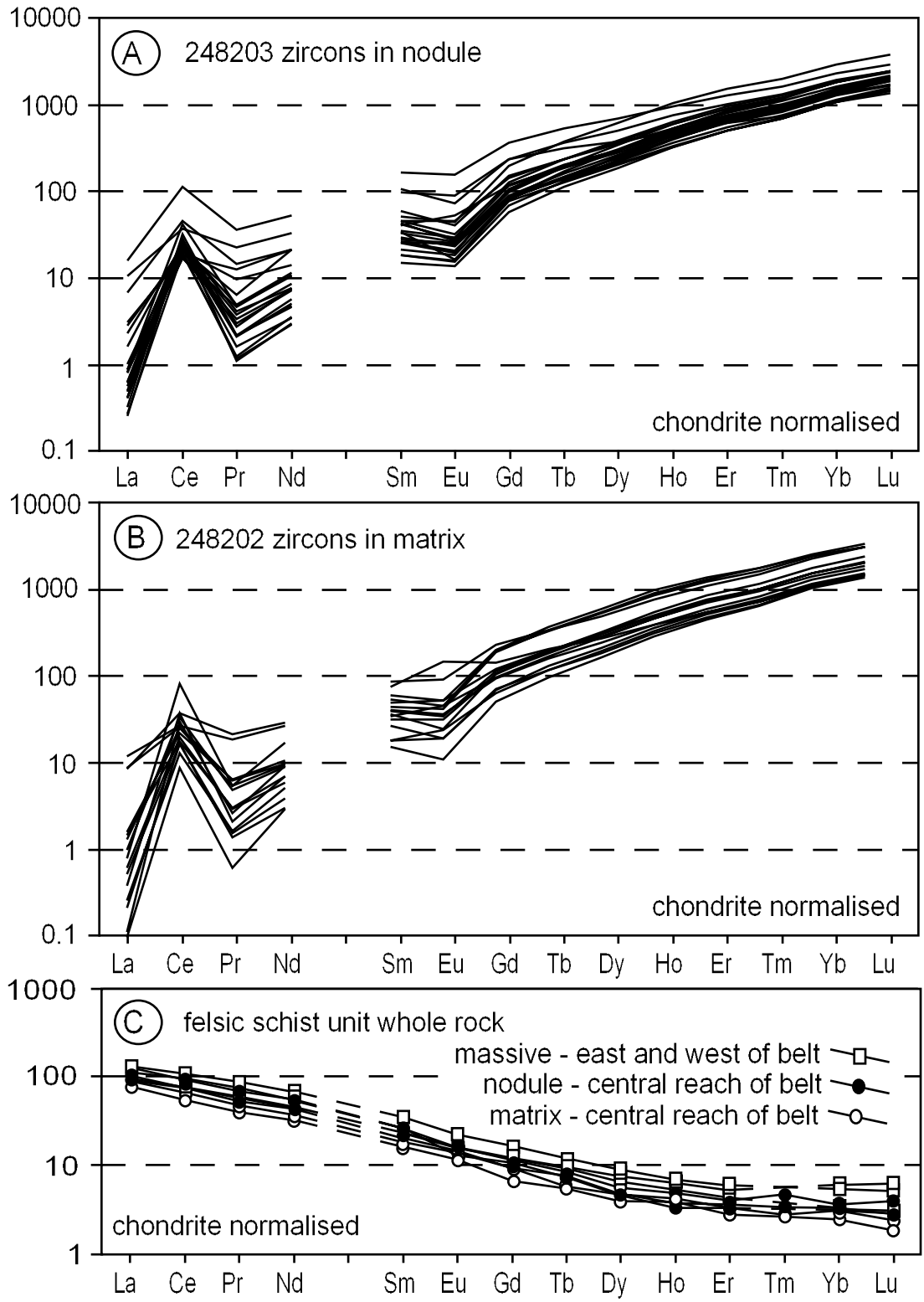
A
248203 zircons in nodule
10000
1000
100
10
1
0.1
chondrite normalised
La Ce Pr Nd Sm Eu Gd Tb Dy Ho Er Tm Yb Lu
B
248202 zircons in matrix
10000
1000
100
10
1
0.1
chondrite normalised
La Ce Pr Nd Sm Eu Gd Tb Dy Ho Er Tm Yb Lu
C
felsic schist unit whole rock
massive - east and west of belt
nodule - central reach of belt
matrix - central reach of belt
1000
100
10
1
chondrite normalised
La Ce Pr Nd Sm Eu Gd Tb Dy Ho Er Tm Yb Lu

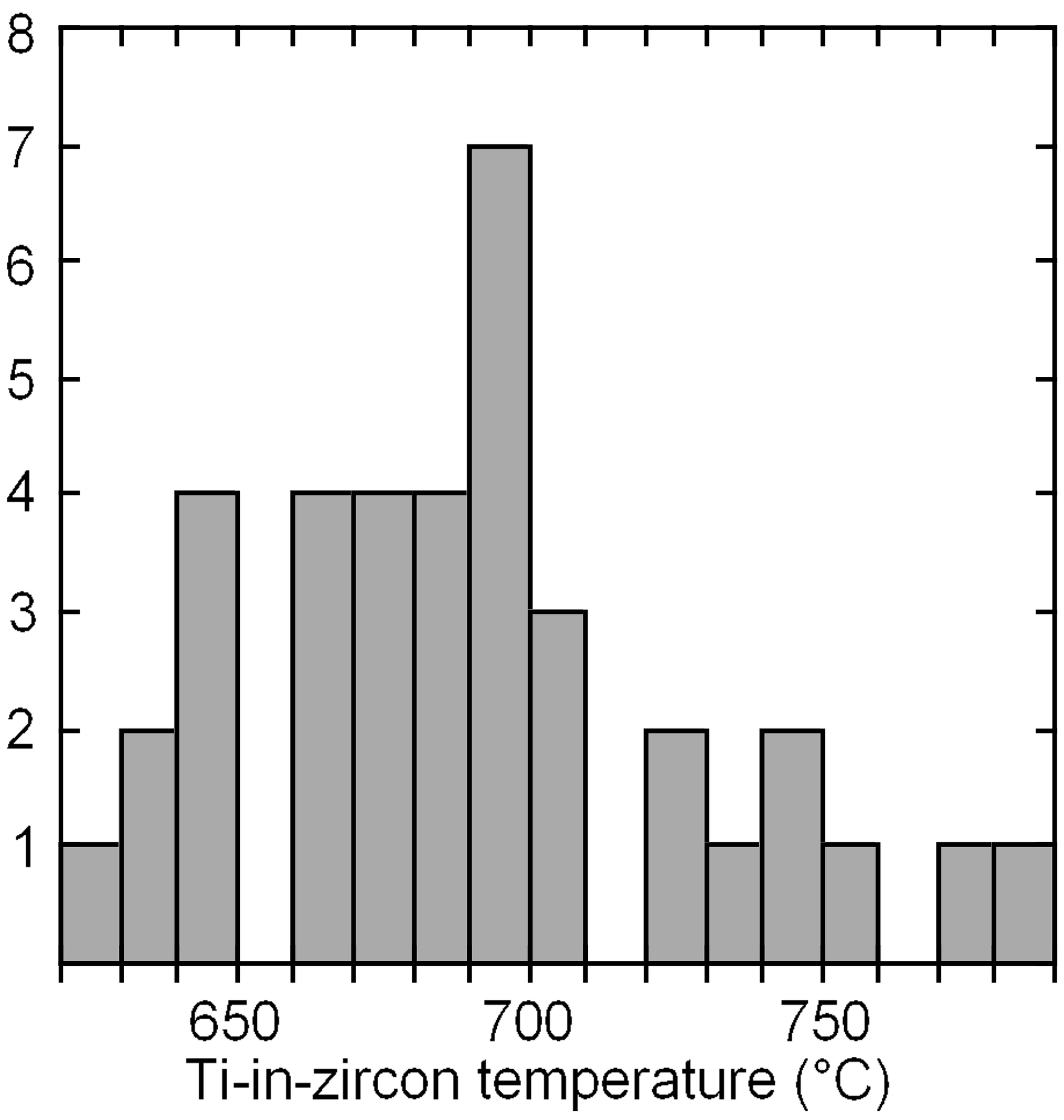
8
7
6
5
4
3
2
1
650
700
750
Ti-in-zircon temperature (°C)

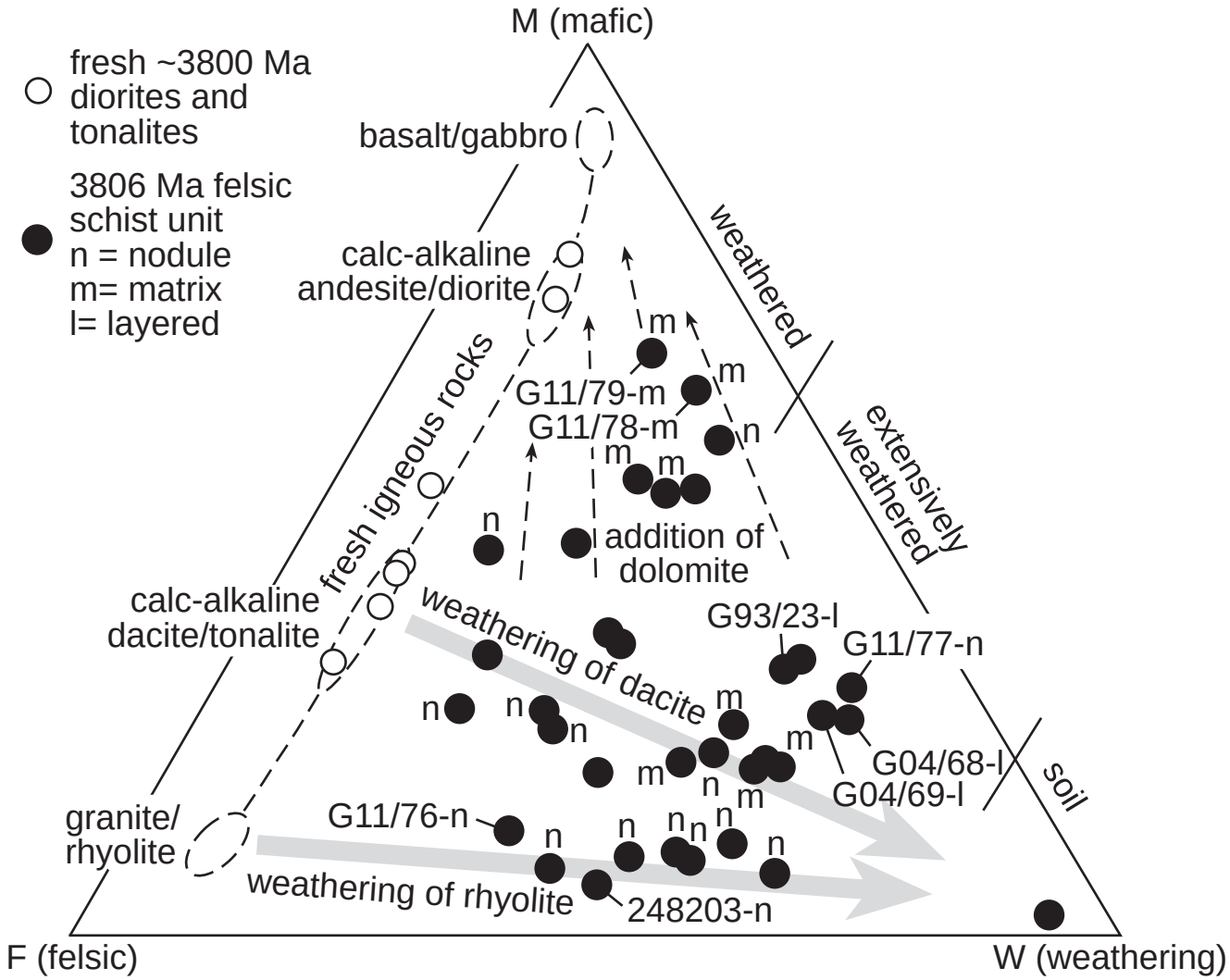
M (mafic)
fresh ~3800 Ma diorites and tonalites
3806 Ma felsic schist unit
n = nodule
m= matrix
l= layered
basalt/gabbro
calc-alkaline andesite/diorite
weathered
extensively weathered
fresh igneous rocks
G11/79-m
G11/78-m
addition of dolomite
calc-alkaline dacite/tonalite
weathering of dacite
G93/23-l
G11/77-n
G04/68-l
G04/69-l
soil
granite/ rhyolite
G11/76-n
weathering of rhyolite
248203-n
F (felsic)
W (weathering)

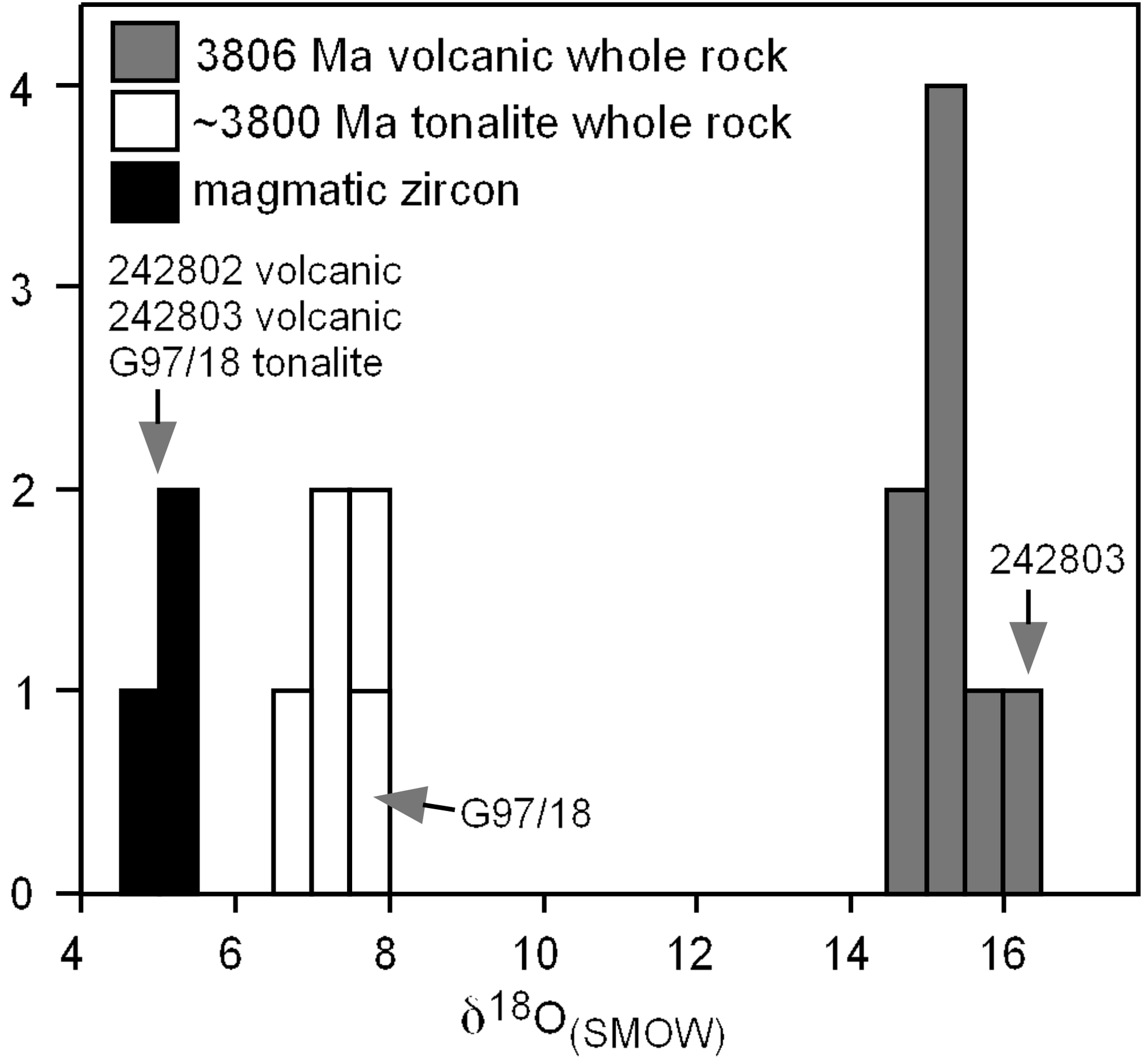
3806 Ma volcanic whole rock
~3800 Ma tonalite whole rock
magmatic zircon
242802 volcanic
242803 volcanic
G97/18 tonalite
242803
G97/18
0
1
2
3
4
4
6
8
10
12
14
16
δ18O(SMOW)

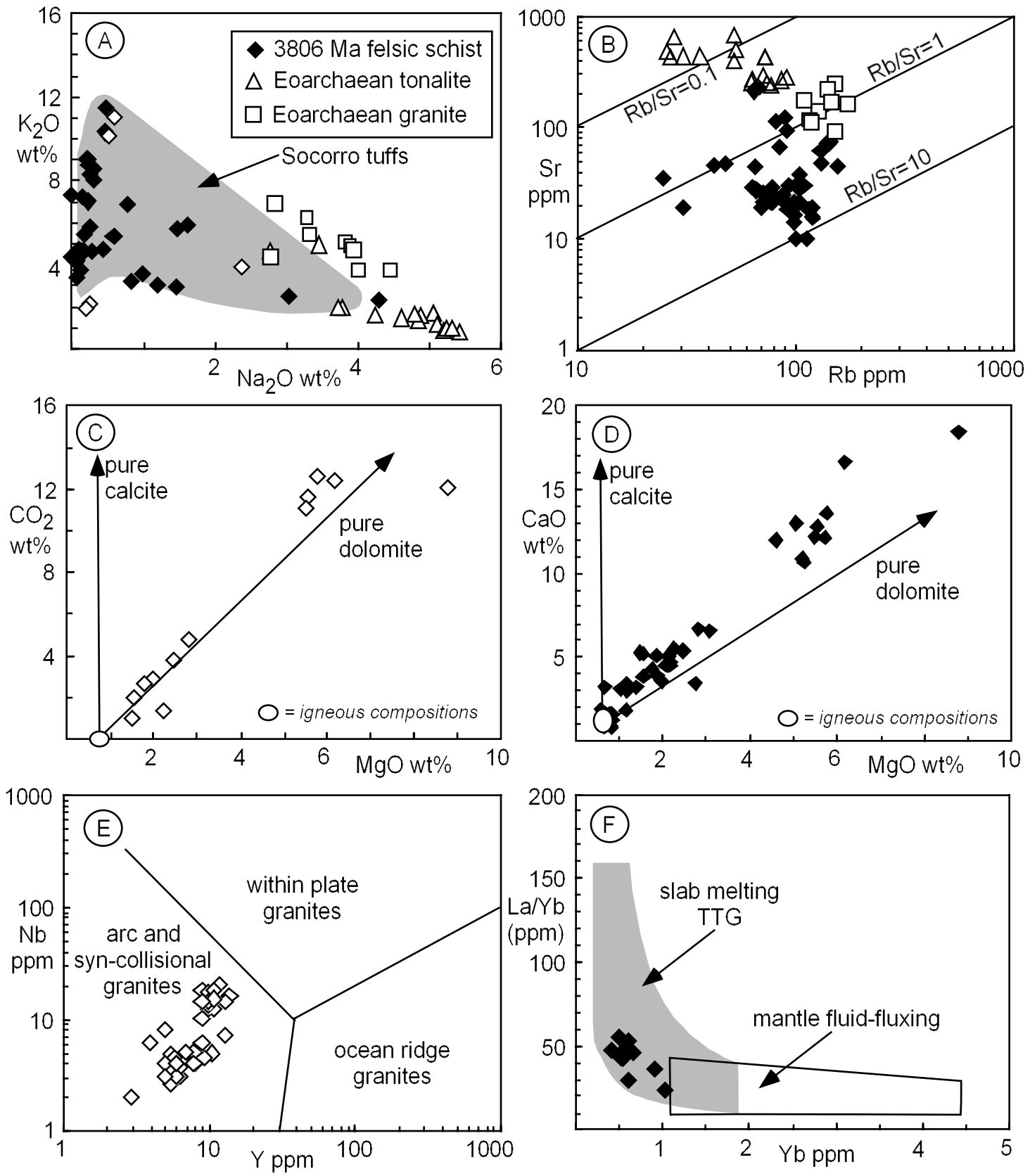
A
3806 Ma felsic schist
Eoarchaean tonalite
Eoarchaean granite
Socorro tuffs
K_2O wt%
Na_2O wt%
B
Rb/Sr=0.1
Rb/Sr=1
Rb/Sr=10
Sr ppm
Rb ppm
C
pure calcite
pure dolomite
= igneous compositions
CO_2 wt%
MgO wt%
D
pure calcite
pure dolomite
= igneous compositions
CaO wt%
MgO wt%
E
within plate granites
arc and syn-collisional granites
ocean ridge granites
Nb ppm
Y ppm
F
slab melting TTG
mantle fluid-fluxing
La/Yb (ppm)
Yb ppm

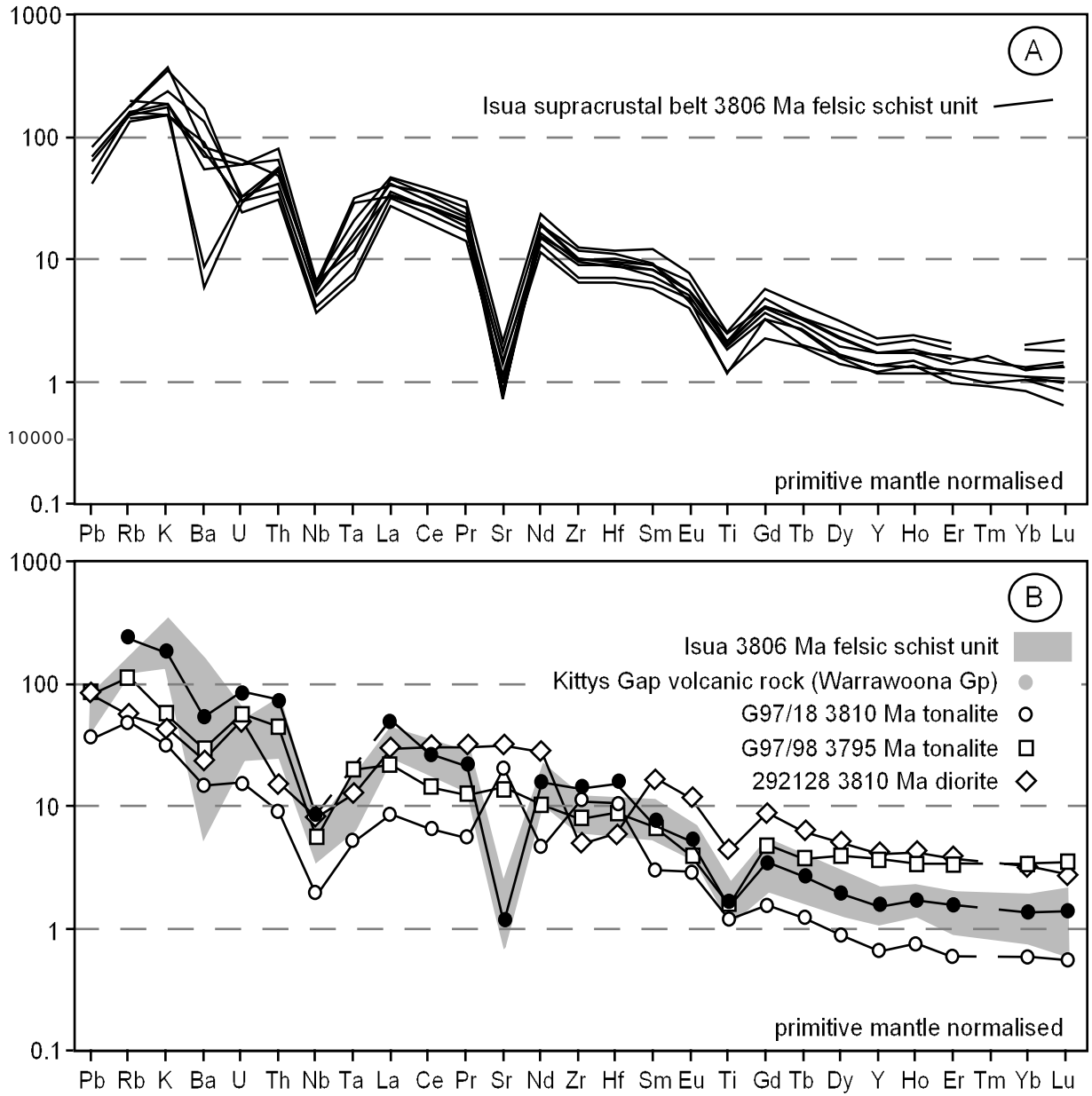
A
Isua supracrustal belt 3806 Ma felsic schist unit
primitive mantle normalised
1000
100
10
1
10000
0.1
Pb Rb K Ba U Th Nb Ta La Ce Pr Sr Nd Zr Hf Sm Eu Ti Gd Tb Dy Y Ho Er Tm Yb Lu
B
Isua 3806 Ma felsic schist unit
Kittys Gap volcanic rock (Warrawoona Gp)
G97/18 3810 Ma tonalite
G97/98 3795 Ma tonalite
292128 3810 Ma diorite
primitive mantle normalised
1000
100
10
1
0.1
Pb Rb K Ba U Th Nb Ta La Ce Pr Sr Nd Zr Hf Sm Eu Ti Gd Tb Dy Y Ho Er Tm Yb Lu

site	description	Ti in zircon (°C)	P	Ti	Th	U	La	Ce	Pr	Nd	Sm	Eu	Gd	Tb	Dy	Ho	Er	Tm	Yb	Lu
248203 nodule zircons																				
1.1	middle with bio (and rut) inclusion	–	300	*58377*	52	107	0.75	11.8	1.21	9.99	6.41	1.68	17.1	5.23	53.2	18.8	83.4	17.8	178	37.1
1.2	end with bio (and rut) inclusion	–	290	*61702*	114	184	0.69	13.4	0.93	6.73	5.25	0.94	15.6	4.81	51.2	18.5	83.2	18.1	179	38.0
10.1	end with bio inclusion	662	298	3.78	70	146	0.07	12.1	0.12	1.68	2.86	0.89	13.9	4.96	57.2	23.0	105	23.0	228	47.9
11.1	middle with bio and ksp inclusion	743	417	9.69	112	168	0.25	14.0	0.37	4.07	6.99	2.65	29.6	8.87	94.6	34.4	149	30.7	301	61.1
12.1	end with ksp and rut inclusion	661	234	3.72	162	221	0.10	14.1	0.16	1.64	3.31	1.07	16.7	5.60	62.5	23.3	103	21.2	210	42.3
12.2	end with ksp and rut inclusion	<639	331	<2.84*	60	118	0.21	11.2	0.32	3.49	4.31	1.49	16.6	5.34	56.7	20.8	91.4	19.5	191	39.9
14.1	end with ksp and bio inclusion	679	422	4.64	123	242	1.68	28.9	1.40	9.97	9.3	2.37	31.3	8.88	89.2	30.4	126	25.9	249	50.1
15.1	edge with rut and qtz inclusion	<647	259	<3.13*	77	143	0.20	10.7	0.45	5.10	6.65	1.57	23.5	6.90	70.7	25.0	107	22.2	217	44.3
16.1	edge with ksp and bio inclusion	690	385	5.31	144	173	0.10	13.4	0.61	10.1	15.1	5.15	48.0	13.6	129	42.5	170	34.0	321	63.1
17.1	edge with rut and bio inclusion	686	408	5.05	125	228	0.20	18.5	0.21	2.20	3.92	1.14	21.8	7.52	86.8	33.7	149	31.0	303	61.8
17.2	edge with rut and bio inclusion	675	206	4.47	97	219	0.06	17.8	0.11	1.44	2.83	0.92	17.4	6.33	76.0	30.7	142	30.7	301	62.1
2.1	edge with tubular void	–	294	*15.0*	87	187	0.15	14.2	0.27	3.63	6.3	3.10	23.9	7.68	76.4	25.7	109	23.1	230	47.7
3.1	end of clean prism	775	301	13.5	127	200	2.59	24.1	2.17	15.5	16.4	4.27	47.3	11.7	96.7	27.6	101	19.0	176	34.2
7.1	end of prism with rut inclusion	699	400	5.94	169	215	0.39	16.3	0.40	3.67	5.01	1.53	21.4	7.10	76.7	28.4	122	25.5	246	49.9
7.2	end of prism with rut inclusion	703	260	6.18	115	180	0.12	15.0	0.21	2.28	4.08	1.42	20.2	7.09	78.9	30.7	134	28.2	274	55.5
8.1	middle with bio and qtz inclusion	740	359	9.42	95	159	0.16	17.2	0.29	3.44	4.48	1.34	18.2	6.02	66.3	25.1	113	24.5	245	51.8
9.1	end clean prism	691	349	5.40	96	174	0.14	14.3	0.20	2.41	4.02	1.21	17.5	5.51	63.6	24.4	112	24.4	241	51.2
9.2	middle clean prism	644	572	3.00	90	151	0.56	15.2	0.48	5.49	7.00	1.88	24.5	7.08	75.5	27.2	118	25.5	251	52.6
A.1	end of broken prism	735	411	8.93	185	260	0.22	26.8	0.46	5.04	7.92	2.60	40.2	14.0	157	59.1	253	51.1	486	96.0
B.1	end of broken prism	<627	202	<2.39*	170	332	0.12	13.0	0.12	1.39	2.32	0.81	11.8	4.22	47.7	18.4	83.7	18.2	182	37.6
C.1	middle of equant grain	–	1006	*27.8*	267	282	3.91	72.4	3.46	24.7	25.3	9.13	74.1	20.1	178	55.0	211	41.2	380	73.6
D.1	middle of equant grain	703	359	6.19	156	239	0.08	20.3	0.21	2.71	5.400	1.72	25.8	8.76	96.9	36.2	157	32.6	312	63.0
248203 matrix zircons																				
13.1	end of homog. grain	632	101	2.54	40	96	0.05	10.6	0.13	1.43	2.34	0.63	10.2	3.54	41.4	15.9	74.1	16.1	167	34.6
13.2	end of homog. grain	690	175	5.35	55	109	0.15	12.5	0.29	2.77	4.11	1.10	14.4	4.30	46.6	17.5	77.9	16.9	172	36.6
18.1	edge by tubular void	667	228	4.02	72	137	0.39	14.0	0.62	4.96	6.18	2.12	19.2	5.84	60.5	21.8	97.0	20.9	209	43.2
18.2	end by tubular void	789	223	15.5	87	137	0.32	16.1	0.52	4.48	5.96	2.00	22.8	7.25	77.7	28.2	124	25.8	249	51.4
19.1	in grain with bio & rut inclusion	685	2254	5.00	89	170	2.09	23.7	2.06	13.8	9.23	3.00	24.2	7.32	72.7	26.3	114	23.8	232	47.1
30.1	end by tubular void	–	255	*95.0*	84	197	2.10	16.2	0.60	4.67	5.20	2.63	19.6	6.35	69.7	26.1	118	25.2	248	51.1
41.1	middle of homog. grain	757	340	11.2	190	161	0.19	52.1	0.52	7.94	13.21	5.30	46.2	12.7	124	42.2	178	37.4	374	78.4
A.1	end of homog. grain	694	327	5.62	196	289	0.24	21.2	0.47	4.28	7.61	3.04	40.0	13.5	149	55.2	224	44.3	405	78.2
A.2	middle of homog. grain	686	388	5.07	85	150	0.06	8.2	0.16	2.43	4.85	1.83	21.4	7.11	80.8	30.9	141	29.6	287	60.3
B.1	end of homog. grain	<640	338	<2.87	82	156	0.35	11.1	0.29	3.31	5.59	1.42	21.7	6.90	75.4	27.6	120	25.2	248	51.0
C.1	in grain with bio & rut inclusion	686	334	5.05	163	203	0.03	18.8	0.25	4.34	8.28	2.65	39.7	12.3	132	47.5	201	41.4	392	78.1
D.1	edge by tubular void	690	364	5.30	59	111	2.90	17.2	1.80	12.7	11.58	8.42	29.3	7.67	67.5	21.8	90.0	18.4	175	36.5
E.1	middle of homog. grain	726	251	8.05	210	253	0.10	23.7	0.20	3.27	6.84	2.38	37.7	12.5	137	49.9	215	43.9	411	82.8
F.1	middle of homog. grain	721	177	7.66	46	104	0.02	5.49	0.06	1.40	2.73	1.10	14.0	4.81	53.5	20.1	89.2	19.1	187	38.6

G.1	end of homog. grain	664	150	3.89	82	168	0.13	10.5	0.15	1.84	2.78	1.36	12.8	4.34	49.1	18.8	84.6	18.1	177	37.0

Ti abundance*; titanium below level of detection. Detection level used to calculate maximum temperature

Sites with very high Ti content (shown in italics) are interprted to contain micro-inclusions, and temperatures are not calculated

bio = biotite, rut = rutile, ksp = potassium feldspar

sample no	G93/24	G93/24	G04/68	G04/69	248203	G11/78	G11/79	G11/76	G11/77	G97/102
protolith	massive	massive	massive	massive	clast	matrix	matrix	clast	clast	mineralised
latitude (N)†		65°05.38'	65°09.464'	65°09.464'		65°05.764'	65°05.764'	65°05.764'	65°05.764'	65°05.25'
longitude (W)		50°09.70'	49°49.957'	49°49.957'		50°00.393'	50°00.393'	50°00.393'	50°00.393'	50°09.07'
zircon age (Ma)					3806 ± 2					3807 ± 6
major elements (wt%)										
SiO_2		62.58	66.45	66.71	68.92	49.57	47.39	62.34	61.25	
TiO_2		0.56	0.45	0.55	0.44	0.26	0.26	0.46	0.40	
Al_2O_3		15.99	14.83	15.24	15.30	8.73	8.48	15.49	12.86	
Fe_2O_3		4.62	3.32	3.35	0.69	5.69	6.32	1.08	3.00	
FeO										
MnO		0.08	0.14	0.16	0.02	0.39	0.43	0.07	0.15	
MgO		2.10	2.19	1.89	0.69	4.61	5.08	0.68	1.88	
CaO		4.47	4.48	3.83	0.84	11.91	12.90	3.16	5.04	
Na_2O		0.27	0.12	0.19	0.58	0.18	0.29	0.47	0.15	
K_2O		5.76	4.71	5.42	11.09	4.64	4.63	11.46	7.16	
P_2O_5		0.22	0.14	0.15	0.18	0.11	0.11	0.23	0.15	
LOI		3.13	3.06	2.40	1.03	12.06	13.49	3.36	5.61	
Total		99.76	99.87	99.90	99.78	98.16	99.37	98.81	97.64	
trace and REE elements (p.p.m.)										
Cr	56	56	47	57	29	47	43	69	43	80
Ni	27					12	10	11	10	
V		69	58	61	43					40
Rb	106	132	95	100	116	88	105	120	99	85
Sr	38	46	30	21	18	24	32	15	16	66
Ba	399	505	64	42	1230	652	540	599	971	221
Y	8.1	10.7	8.1	9.3	5.5	5.5	6.4	8.1	6.4	5.9
Pb	13.41					7.83	9.62	15.7	12.22	600
Zr	115	146.4	117.5	110.5	137.7	73.9	80.5	115.9	102.9	139.0
Hf	3.23	3.79	2.94	2.77	3.52	2.05	2.23	3.06	2.84	3.6
Nb	4.01	4.90	4.35	4.41	4.71	2.63	3.01	4.92	3.7	4.4
Ta	0.69	0.88	1.22	0.62	1.34	0.29	0.32	0.50	0.46	0.40
Th	5.82	7.13	4.93	4.65	4.79	2.68	3.15	4.29	3.60	5.43
U	1.30	1.31	0.71	0.63	0.66	0.53	0.66	1.40	0.70	1.42
La	29.7	33.2	23.1	24.2	28.6	19.6	22.6	32.2	25.8	18.1
Ce	54.1	70.7	49.0	50.4	63.3	36.1	43.4	61.3	49.0	35.0
Pr	6.24	8.65	5.74	5.90	7.48	3.98	4.74	6.77	5.28	4.08
Nd	26.7	33.2	21.7	22.5	26.8	15.9	18.3	27.0	21.2	14.8
Sm	4.10	5.60	3.69	3.77	4.23	2.59	2.90	4.13	3.28	2.35
Eu	1.16	1.34	0.94	0.96	0.77	0.69	0.83	0.96	0.88	0.52
Gd	2.93	3.51	2.51	2.54	2.24	1.40	1.97	2.43	1.97	1.61
Tb	0.368	0.470	0.362	0.369	0.286	0.214	0.224	0.329	0.297	0.210
Dy	1.75	2.34	1.71	1.99	1.20	1.04	1.23	1.46	1.26	0.96
Ho	0.287	0.406	0.309	0.371	0.195	0.226	0.247	0.286	0.218	0.210
Er	0.80	1.01	0.74	0.90	0.56	0.48	0.56	0.69	0.61	0.63
Tm	0.110					0.070	0.074	0.124	0.088	0.090
Yb	0.674	0.923	0.547	1.022	0.521	0.418	0.526	0.614	0.558	0.620
Lu	0.108	0.134	0.080	0.164	0.076	0.049	0.063	0.103	0.074	0.090

majors	GA	GA	GA	GA	GA	UW	UW	UW	UW	UW
trace and RE	QUT, UW	ANU, GA	ANU, GA	ANU, GA	ANU, GA	QUT, UW	QUT, UW	QUT, UW	QUT, UW	QUT, UW

† positions referenced to WGS84

Analytical laboratories; UW = University of Wollongong; QUT = Queensland University of Technology;
ANU = Australian National University; GA = Geoscience Australia

sample	source	type	$\delta^{18}O_{VSMOW}$ ‰
G93/24	a	felsic schist	14.7
G04/68	a	felsic schist	15.1
G04/69	a	felsic schist	14.6
G11/76	a	nodule	15.8
G11/77	a	nodule	15.4
G11/78	a	matrix	15.3
G11/79	a	matrix	15.0
248203	a	nodule	16.2
G97/18	a	tonalite	7.8
225926	b	pegmatite	2.0
229472	b	pegmatite	8.7
229405	b	pegmatite	9.2
225841	b	tonalite	7.3
225858	b	tonalite	6.5
225942	b	tonalite	7.5
225943	b	tonalite	7.3